André Castanheira Lourenço

Licenciado em Engenharia de Micro e Nanotecnologias

Sunlight-driven CO_2-to-fuel conversion: exploring thermal and electrical coupling between photovoltaic and electrochemical systems for optimum solar-methane production

Dissertação para obtenção do Grau de Mestre em

Engenharia de Micro e Nanotecnologias

Orientador: Manuel J. Mendes, Professor Assistente,
Faculdade de ciências e tecnologias, Universidade NOVA de Lisboa

Co-orientador: Doutora Ana Reis Machado, Investigadora Auxiliar,
Faculdade de ciências e tecnologias, Universidade NOVA de Lisboa

Júri:

Presidente: Doutor Luís Miguel Nunes Pereira

Arguente: Doutor Carlos Manuel Faria de Barros Henriques

Vogal: Doutor Manuel João de Moura Dias Mendes

FACULDADE DE CIÊNCIAS E TECNOLOGIA
UNIVERSIDADE NOVA DE LISBOA

Outubro, 2019

Sunlight-driven CO_2-to-fuel conversion: exploring thermal and electrical coupling between photovoltaic and electrochemical systems for optimum solar-methane production

Acknowledgments

Em primeiro lugar gostaria de agradecer ao Professor Doutor Rodrigo Martins, como presidente do Departamento de Ciência dos Materiais, e à Professora Doutora Elvira Fortunato, como Diretora do Centro de Investigação de Materiais, por todo o apoio e dedicação do DCM, CENIMAT e do curso de Engenharia de Micro e Nanotecnologias, que me permitiram crescer e formar como pessoa nos últimos 5 anos. Um agradecimento especial ao Prof. Manuel J. Mendes, meu orientador, e à Dra. Ana Reis Machado, minha coorientadora, pela oportunidade de trabalhar neste tema inovador e pela ajuda prestada sempre que a solicitei.

Quero agradecer também ao DCM e a todos os professores que me habilitaram com as ferramentas necessárias que me tornaram num engenheiro.

Um muito obrigado aos colegas de curso, em especial ao meu grupo mais próximo, Pedro, Carlos e Jorge, que tornaram tudo mais fácil, mas também ao Fábio Vieira que, já tendo trabalhado neste tema, se mostrou sempre disponível para me ajudar.

Finalmente agradecimento à minha família por todo o apoio.

Abstract

Artificial photosynthesis is regarded as the best way to protect the environment while producing carbon-based fuels, because it closes the anthropogenic carbon cycle. Herein we simulate a Photovoltaics-Electrochemical (PV-EC) system capable of converting CO_2 into usable carbon-based fuels, in order to analyse the implementation of synergetic techniques such as intermediate electronic regulation and thermal coupling on the improvement of the energetic performance. We proved that, when thermally coupled, the two cells of the system exhibit a symbiotic behaviour: the solar-to-fuel efficiency stays almost temperature-independent due to improved reaction kinetics which compensates for photovoltaic thermal losses. The electronic regulation is equally important to enhance efficiency because it guarantees that we make use of the full PV power output to the EC load. These solutions are tested in two pathways for methane production: 1-step, $CO_2 \rightarrow CH_4$, and 2-step, $CO_2 \rightarrow Syngas \rightarrow CH_4$, exhibiting solar-to-fuel efficiency gains up to 586% and 43%, respectively, when compared with the systems without both the thermal coupling and the DC-to-DC converter. Lastly, an energetic comparison of the two pathways was made. The direct production (1-step) of methane showed to provide 20% less energy than the second path, where syngas is produced and converted to methane through a Fischer-Tropsch synthesis at 350 °C and 10 atm.

Keywords: Artificial Photosynthesis, Solar-powered Fuel synthesis; CO_2 Electrochemical reduction; Photovoltaic-Electrochemistry Thermal coupling; DC-to-DC converter; Fischer-Tropsch synthesis; Analytical Modelling of Solar Fuel generation

Resumo

A fotossíntese artificial é considerada a melhor maneira de proteger o ambiente enquanto se produz combustíveis à base de carbono porque fecha o ciclo antropogénico do carbono. Neste trabalho simulamos um sistema Fotovoltaico-Eletroquímico (PV-EC) capaz de converter CO_2 em combustíveis usáveis à base de carbono, de maneira a analisar a implementação de técnicas sinergéticas, como é o caso da regulação eletrónica e o acoplamento térmico, na melhoria de performance do sistema. Provou-se que quando o sistema está termicamente acoplado as duas células exibem um comportamento simbiótico: a eficiência fica praticamente independente da temperatura devido às melhorias na cinética da reação, que vão compensar as perdas térmicas do fotovoltaico. A regulação eletrónica é igualmente importante no aumento da eficiência porque garante que conseguimos usar toda a energia fornecida pelo PV no favorecimento da reação eletroquímica. Estas soluções são testadas em dois métodos alternativos para a produção de metano: processo a 1-passo, CO2→CH4, e a 2-passos, CO2→Syngas→CH4, exibindo ganhos na eficiência total de 586% e 43%, respetivamente, comparando com o sistema sem acoplamento térmico nem usando conversor de DC-para-DC. Por fim a comparação energética dos dois métodos foi feita. A produção direta de metano (processo a 1-passo) mostrou ser 20% menos energética que a outra alternativa, onde o gás de síntese é produzido e convertido em metano através do processo de Fischer-Tropsch nas condições de 350 °C e 10 atm.

Palavras-Chave: Fotossíntese Artificial; Produção de combustível usando energia solar; Célula Eletroquímica alimentada por energia solar; Redução eletroquímica de CO_2; Acoplamento térmico Fotovoltaico-Eletroquímico; Conversor DC-para-DC; Síntese de Fischer-Tropsch; Modelação analítica da produção de combustível usando energia solar;

Contents

List of Figures

List of tables

Symbols

γ	Linear parameter
AM	Air mass Coefficient
E^0	Thermodynamic cell potential (V)
I_0	Saturation current (A)
I_{ph}	Light generated current (A)
I_{sc}	Short-circuit current (A)
J_0	Exchange current density ($mA \cdot cm^{-2}$)
J_0^{ref}	Current density at the reference temperature ($mA \cdot cm^{-2}$)
K_B	Boltzmann constant ($J \cdot K^{-1}$)
m_i	Mass of the specie i (g)
M_i	Molar mass of species i ($g \cdot mol^{-1}$)
N_s	Number of solar cells in series
P_i	Pressure at the condition i
R_p	Shunt resistance (Ω)
R_s	Series resistance (Ω)
s_i	Stoichiometric coefficient of this specie i
T_{ref}	Reference Temperature (K)
V_i	Volume at the condition i
V_{op}	Operational voltage (V)
V_T	Thermal voltage (V)
α_a	Anodic transfer coefficient
α_c	Cathodic transfer coefficient
η_{EC}	Electrochemical efficiency

η_d	diode ideality/quality factor
C	Specific heat (kJ·Kg^{-1}·K)
E	Cell potential (V)
Ea	Activation energy (J·mol^{-1})
F	Faraday's constant (C·mol^{-1})
G	Solar irradiance (W·m^{-2})
I	Working current (A)
J	Current density (mA·cm^{-2})
m	Exponent parameter
n	Number of electrons involved in the reaction
q	Electronic charge (C)
Q	Heat (J)
R	Gas constant (J·K^{-1}·mol^{-1})
T	Working temperature (K)
t	Production time (s)
V	Applied voltage (V)
ΔH	Enthalpy variation (kJ·mol^{-1})
ΔS	Entropy variation between products and reactants (kJ·mol^{-1})
η	Overpotential (V)

Acronyms

PV	Photovoltaic
EC	Electrochemical
PEC	Photoelectrochemical
FTS	Fischer-Tropsch Synthesis
FT	Fischer-Tropsch
SPE	Solid Polymer Electrolyte
MEA	Membrane Electrode Assembly
Mono-Si	Monocrystalline Silicone
GDL	Gas Diffusion Layer
CO2RR	CO_2 Reduction Reaction
GHG	Greenhouse Gas
SHE	Standard Hydrogen Electrode
EE	Electric Efficiency
RHE	Reversible Hydrogen Electrode
MPP	Maximum Power Point
OP	Operating Point
TC	Thermal Coupling
NoTC	No Thermal Coupling
EE_{PV}	Solar-to-electricity efficiency
EE	Electrochemical Efficiency
POAR	Power Over Area Ratio
DCDC	DC-to-DC converter
LHV	Lower Heating Value or net calorific value
FF	Fill Factor

Motivation and Objectives

The increasing demand for energy, which followed the industrial revolution and world's population increase, favours the continuous use of fossil fuels, since this is a mature energy source, the technologies for its exploitation are also mature and yields excellent energy vectors (natural gas, gasoline, diesel). However, such increasing demand stresses our planet with the ever-increasing greenhouse gas emissions, which calls for more environmentally friendly approaches. Solar energy is in a good place to replace the fossil fuels, not only because exploiting only 0.01% of the total solar power that reaches Earth would be enough to cover the global consumption, but also because this technology is now reaching a point of maturity where the cost per kWh (after diminishing in the last decades) is now close to the cost from the grid. Unfortunately, problems regarding its intermittency, storage and transport have slowed the deployment of this technology. By getting the best of the two worlds, artificial photosynthesis shows to be a better approach, as Figure 1 depicts [1]. It combines a solar harvesting mechanism (photovoltaics) with a chemical "reactor" (electrochemical cell) to produce carbon-based fuels (i.e. solar fuels) from solar energy, water and even from gas emissions (e.g. CO2 captured from exhaust as the carbon source). This way, it will still be possible to satisfy the energetic demand for the next decades without increasing the amount of greenhouse gases in the atmosphere. This work aims to module and study this type of process: to understand the best way to integrate the two systems, how temperature influences production and if it is possible to place a system like this in everyone's homes. Methane production will be the main purpose of our study since it is widely used in building applications, which are the leading energy consumers in Europe (40%) [2], [3].

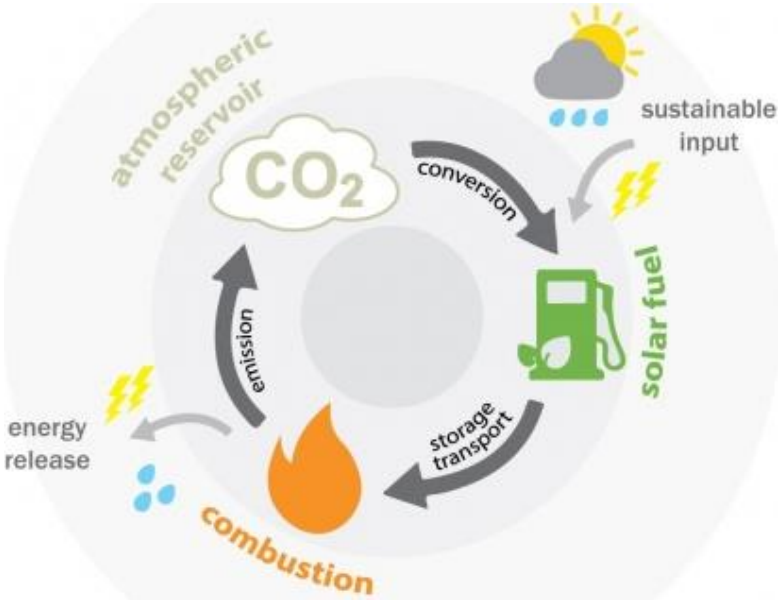

Figure 1 – solar fuels production cycle. Water, CO_2 and solar energy as input are transformed into solar fuels that can be used as energy sources [1].

1 Introduction

The present energetic and environmental issues that we are facing in a global scale have shown that the future of our society's primary power source should be clean and renewable, such as wind and solar energies. However, despite the *energy per hour* provided by those sources being more than enough to our yearly necessities (~16 TW) [4], the mechanisms to extract power from them are not yet efficient enough to surpass the carbon-based fuels. Moreover, the lack of cost-effective technologies (normally batteries) to store their intermittent power supplies makes the energy difficult to transport and distribute (i.e. providing solar converted electricity to a country with low solar irradiance would be difficult). Also, fuels allow much higher density (e.g. ~50 $MJ \cdot Kg^{-1}$ for Natural Gas) than batteries (~1 $MJ \cdot Kg^{-1}$ for advanced Li-batteries) and does not degrades as fast [5]. Therefore, nowadays, we still depend too much on Carbon-based fuels which magnifies the global warming problem. In Europe, for example, buildings are responsible for the highest energetic consumptions and carbonic footprint (40%). From it, 79% is due to the space heating and hot water provision, which are mainly generated from fossil fuels-based energy sources (84% - only 16% use of renewable energies) [2], [3].

Thus, once carbon-based fuels will remain in our lives for the next decades, one can find sustainable ways to produce and even reutilize them. That is the aim of this work: to use sunlight to power processes that contribute to the reduction of CO_2 emissions and transform it into usable carbon-based gases/fuels. An idea as novel and sustainable as a CO_2 recycling mechanism using solar energy could mitigate the current energetic and environmental issues for the well-being of future generations.

Fuels generated by artificial photosynthesis processes, also known as solar-fuels, are in the base of such ideas. It relies in a combination of a Photovoltaic (PV) system and CO_2 flow of gas to feed an electrochemical (EC) system that synthesises the required carbon-based fuel. In an alternative approach, photoelectrochemical (PEC) devices, have the photoabsorber/photovoltaic material directly in contact with the catalyst and inside the electrolyte. Although being a more compact approach with a single device, this leads to excessive exposure of the semiconductor and consequent fast degradation [6], [7]. Consequently, PV-EC systems which simply integrate separate PV and EC components are a better solution, not only from the point of view of longevity but also for optimization purposes since we can trim both systems independently. As such, in this work we will focus on PV-EC systems.

This thesis will mainly focus on the production of CH_4 since it is the main constituent of Natural Gas, which gathers a set of important characteristics: (1) has high energy density, ~50 $MJ \cdot Kg^{-1}$; (2) it is a conceptually simple, easy-to-obtain hydrocarbon; (3) infrastructures for its use and storage are already in place; (4) has many uses in our society, mainly at the residential level which is the main cause for the carbonic footprint. As such, a cleaner methane production process would create a higher impact in our society, in comparison with other fuels. We compared methane production from two different routes: 1) by a direct EC production (1-step process), and 2) via the synthesis of syngas intermediate followed by a Fischer-Tropsch (FTS) reaction (2-step process), both presented in Figure 1.1. The electrochemical reactions involving these processes are the following [5]:

Syngas production reactions:

$$CO_2 + H_2O \rightleftharpoons \mathbf{CO} + H_2O + \tfrac{1}{2}O_2 \quad (1)$$

$$2H_2O \rightleftharpoons 2\mathbf{H_2} + O_2 \quad (2)$$

Methane production reaction:

$$CO_2 + 2H_2O \rightleftharpoons \mathbf{CH_4} + 2O_2 \quad (3)$$

Simulations will be made considering a Solid Polymer Electrolyte (SPE) in a Membrane Electrode Assembly (MEA) that can directly produce methane or syngas (that is, a combination of CO and H_2) at tunable ratios, allowing further transformation of products in usable fuels. Our EC components were based on the most state-of-the-art papers that we could find in literature [8], [9], and the PV systems were simulated according to both commercially available solar Monocrystalline-Silicone (mono-Si) cells (SUNPOWER – datasheet presented in Appendix I) and an advanced, close to theoretical limits, Perovskite/Silicon tandem cell (which we always refer as Perovskite/Si cell). The latter uses a double junction which allows for efficiency improvements. The high bandgap Perovskite top sub-cell absorbs high energy photons (from UV and Visible spectrum) while the bottom Silicon sub-cell makes use of the remaining visible and near-infrared light. Light trapping is also considered, which improves the amount of light converted in photonic solutions [10]–[13]. For 1000 $W \cdot m^{-2}$, AM (air mass coefficient) of 1.5G irradiation(1-Sun) and 298 K this cell has an open-circuit voltage of 1.45 V and a short-circuit current of 28.9 $mA \cdot cm^{-2}$, giving an efficiency of 30.9 %.

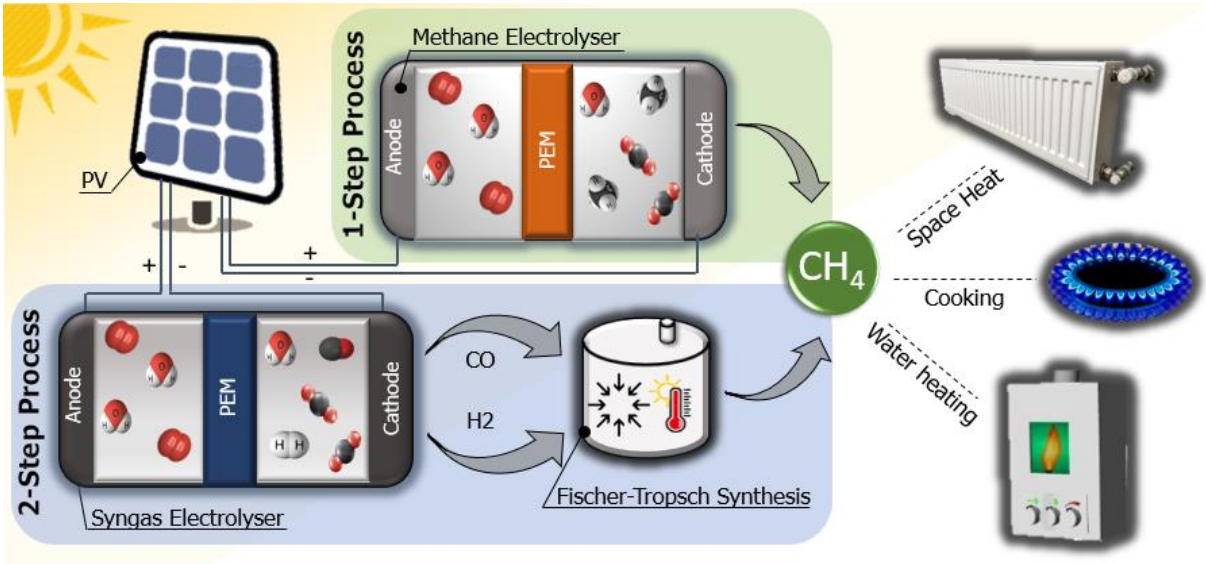

Figure 1.1 – Photovoltaic-powered paths of reaction studied to obtain methane from CO_2 and water. The top scheme is the 1-step reaction, where methane is obtained right after the EC process. The bottom path is the 2-step process, which requires two reactions: a first one that produces an intermediate product called syngas (combination of CO and H_2), and a second (FT synthesis) that from syngas, using high temperature and pressure, obtains methane. The picture also shows some consumer applications for the "solar methane" produced.

1.1 Electrochemical considerations

Over the years many efforts have been made in this field which makes possible to identify key factors for a successful, affordable and efficient EC system [6], [14], [15]: *(a)* Temperature; *(b)* Pressure; *(c)* pH;

(d) Electrodes and catalyst constitution (activity and selectivity); *(e)* Overpotentials; *(f)* Type of electrolyte and assembly; (g) electrochemical cell design; *(h)* stability over time; *(i)* Economic viability.

Usually high temperature and pressure facilitates the chemical reaction but require a more robust and less affordable apparatus. However, the higher costs of working at higher pressure may be compensated by increased energy efficiencies, due to minimization of intermediate compression steps and the direct coupling of downstream high pressure processes [16], [17]. The use of different electrodes and catalysts could influence both the overpotential of the process, sometimes making it more energetically consuming, and the pathway of the reaction, outputting different products such as methane (CH_4), ethanol (CH_3CH_2OH), carbon monoxide (CO), hydrogen (H_2) and other compounds (e.g. Ag and Zn for CO, Cu for CH_4, Ni for H_2) [18]. The control of pH, as performed by Masel et al. [19], allows for a very high tunability of the cell's products but requires a watertight cell design is neither the most efficient nor convenient. Moreover, the change of cell design brought significant improvements. Instead of using the typical "H-cell" design, researchers started using flow cells that allowed constant circulation of products and reactants, reducing previous limitations with mass transportation [15]. Some works also refer that the removal of liquid electrolytes is beneficial. Liquid electrolytes necessitate a first diffusion of CO_2 before the reaction can occur, but CO_2 has low solubility limits in aqueous media (current density limited to 30 $mA \cdot cm^{-2}$). Instead, a flow of hydrated carbon dioxide reacts in the gas phase [15], [20].

Accordingly, the migration to structures of the type membrane electrode assembly (MEA) assisted by gas diffusion layers (GDL), as shown in Figure 1.2, to facilitate the flow of elements permits reaching much higher current densities (around 200 $mA \cdot cm^{-2}$) in the CO_2 reduction reaction (CO2RR).Many works have been undertaken in the past decades related with the production of H_2 from PV-EC, since it is an easy product to obtain and the process can easily reach 100% selectivity, but H2 is a highly volatile gas which is hard to safely store and transport. So, other products are more promising, which are the cases of CH_4 and syngas. Syngas is a combination of CO and H_2 and is very useful as an intermediate product, as it is quite versatile, normally used to obtain other hydrocarbons like CH_4 by the Fischer-Tropsch (FTS) process [21]–[27]. Exploring the production of CH_4 is also very important because, as mentioned before, heat provision in buildings is presently the most energy-consuming activity in developed countries, and it depends mostly on CH_4 (Natural Gas) [28], [29]. Also, its demand will increase since Europe intends to reduce greenhouse gas (GHG) emissions by 80% to 95% by 2050, and it is only possible to do so through replacing current heating systems by gas-based ones [28]. Being able to produce it from a sustainable process could be an important step to reduce our environmental footprint even faster.

1.2 Photovoltaic and Electrolyser integration

There are several important aspects to take into consideration when connecting two independent PV & EC systems. Firstly, we must guarantee that both systems are state-of-the-art so they can have the highest efficiencies possible. Secondly, the connection must have minimum losses and the working point must be wisely chosen so we can transfer all the power obtained by the PV system to the EC cell. This tuning can be achieved either by manipulating the ratio of areas of the two parts, and/or simply by implementing a DC-DC converter. This way we guarantee that the full power provided by the PV is provided to the EC load, in order to produce the

highest possible quantity of products. Finally, we benefit from symbiotic behaviour when integrating/connecting both systems. As it is well known, solar cells lose efficiency for increasing temperatures. On the other hand, the EC reactions considered in this work are endothermic processes ($\Delta H > 0$), meaning that temperature increases favour the yield of products (Le Chatelier's Principle). Consequently, by thermally coupling both systems, it is possible to achieve higher efficiencies and more stability over a wide temperature range. Our results will show that the efficiency variations can go up to 29% when the systems are not coupled. These results support the idea of building a compact system to be implemented on the rooftop, as sketched in Figure 1.2. This strategy will turn the disadvantages of individual systems into competitive advantages of the system under study.

Previous works have addressed similar aspects, but not as performed in this work. In our we try to complement previous experimental works - that normally only focuses one element of the PV-EC system that we discussed before (either PV or EC or integration or implementation) - by analysing the state-of-the-art systems from all the perspectives in order to anticipate a real-life application. For example, Schreier et al. [14] created a PEC system with liquid electrolyte that could reach 13.4% of efficiency but misses an analysis on the implementation. Other

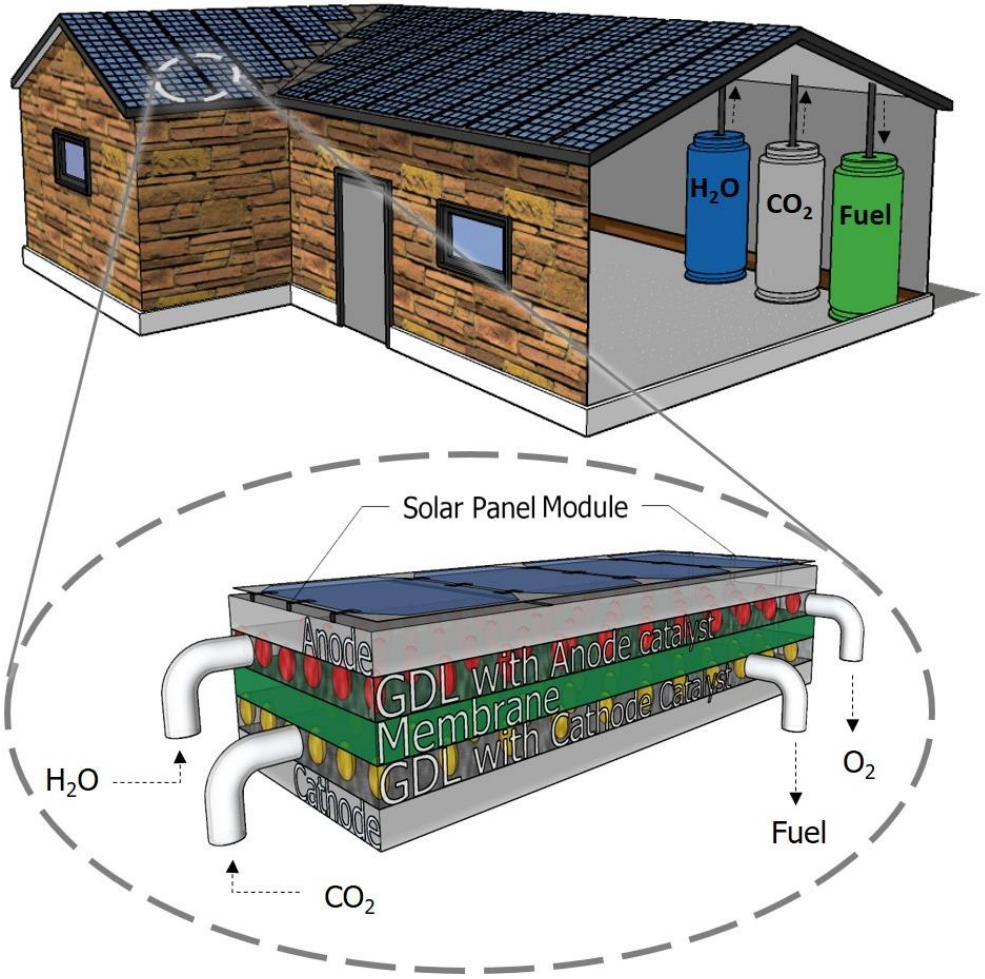

Figure 1.2 – Representation of a possible implementation of the integrated PV-EC system (i.e. EC integrated beneath solar panels, on the house's roof). The attachment of the EC cells to the rear of the solar cells allow thermal coupling between the PV and EC for better combined performance. The close-up of the PV-EC system shows the assembly: EC system based on PEM and MEA assembly, without liquid electrolyte and with catalysts, for selectivity improvements. The gas inlets and outlets are connected to gas bottles inside the house.

work developed at our centre [27] with the same intentions as us, shows efficiency of 13.26% but without the stability over the temperature range that we manage to have and without obtaining the solar-to-fuel efficiencies of 18% that we manage to reach.

1.3 Fischer-Tropsch synthesis

To compare the two processes depicted in Figure 1.1, it is important to analyse them not only from the production point of view (efficiency and mass of gas supplied), but also from the energetic balance point of view. Taking another look to Figure 1.1, in the 1-step process the output can be directly used for consumption while the second path needs syngas conversion by the Fischer-Tropsch process which will require some energy input besides gases. The methanation reaction is the following [25]:

$$CO + 3H_2 \rightleftharpoons \mathbf{CH_4} + H_2O \quad (4)$$

It relies on the manipulation of Temperature, Pressure, proportion of input gas(es) and catalyst constitution to form the desired hydrocarbons, since they control the degree of polymerization and the distribution of products [26].From the thermodynamic point of view, we can conclude that low temperature, high pressure and precise CO:H_2 proportion (3:1, in this case) facilitates the reaction. However, the reaction requires catalysts to promote the reaction and avoid the production of unwanted by-products. Catalysts are not as active at low temperatures as they are at high temperatures, making very-low temperature (below 300 °C) FTS process a challenge [23]. Also, every catalyst will behave differently, so it is not only important to consider its activity but also its selectivity towards methanation. Important metals for the methanation process have been found to be Ru, Ni, Co, Fe and Mo which can be compared as follows [22], [25]:

Activity: Ru > Fe > Ni > Co > Mo

Selectivity: Ni > Co > Fe > Ru

The most desirable metals are ruthenium and iron, due to their relatively high activity and low price, respectively. However, cost and low selectivity in the first case and selectivity in the second, make them unsuitable for direct use without proper filtering. Molybdenum shows low activity and is more selective towards C_{2+} hydrocarbons, which we want to avoid. Between Nickel and Cobalt, Ni takes advantage in all factors, meaning it is the most adequate metal for the methanation process. Also, Ni performance can be improved by increasing the pressure [22].Gao et al. [23] performed a thermodynamic study that showed around 100% efficiency for CH_4 production from syngas (at 350 °C and above 10 atm), results that comply with the selectivity and yield of some commercially available products using Ni catalysts. We have used these results in our analysis. Despite syngas having higher production efficiencies, as shown in our results and studied literature [8], [9], the final FTS efficiency and power consumption can greatly influence the 2-step results. Herein we provide an estimation of the energetic cost of FTS process and compare the two possible paths of Figure 1.1 to see which one is more viable.

2 Methods and Model Description

The simulations studies performed in this thesis were based on state-of-the-art experimental data concerning previous published experimental works or on products available in the market, which we describe in section 3. The reactions kinetics, PV models and efficiency assessment formulas necessary to model those datasets are presented in this section. The models presented here were computed for further study using Origin and Wolfram Mathematica Software. The former was very useful for plotting and adjusting the models to the datasets, while the latter, an analytical calculation and simulation tool, was important in the manipulation of the models to, using programming skills, estimate the desired results.

2.1 Electrochemical model

In fuel cells the working principles are redox reactions. For this type of reaction, we can have either galvanic cells (electrochemical cells of which batteries are an example) and electrolytic cells. The former ones occur spontaneously and correspond to the inverse reaction of the latter ones. The reactions we are working with are electrolytic, so we need to apply a potential difference to start the process. The relation between the total current and the applied potential can be described by the Butler-Volmer equation [18], [20], [27], [30]–[34]:

$$J = J_0 \times \left(\exp\left(\frac{\alpha_a F(V - \eta - E)}{RT} \right) - \exp\left(\frac{\alpha_c F(V - \eta - E)}{RT} \right) \right) \quad (5)$$

Where J is the reactor current density (mA·cm^{-2}), J_0 is the exchange current density (mA·cm^{-2}), T is the Temperature (K), V corresponds to the applied voltage (V), R and F are two constants which represent, respectively, the constant of gases (8.3144 J·K^{-1}·mol^{-1}) and Faraday's constant (96485 C·mol^{-1}), α_a and α_c are, accordingly, the anodic and cathodic transfer coefficients and define how the potential influences each side of the reaction in relation to the other. η are the overpotentials (V). As the name suggests, it is a parameter that includes all the phenomena that make the working voltage value higher than the thermodynamic cell potential (E^0). It includes mass transport overpotential, ohmic overpotential and other assembly and material related overpotentials [33]. The cell potential, E, depends on the thermodynamic cell potential (E^0), which corresponds to the theoretical potential value at which the reaction should start, and its value is given by the following formula:

$$E^0 = \frac{T\Delta S - \Delta H}{nF} \quad (6)$$

Where ΔS and ΔH are, respectively, the entropy and enthalpy variations between products and reagents (in kJ·mol^{-1}) and n is the number of electrons involved in the reaction. These values depend on the reaction type: the corresponding values for each reaction in study are present in Table 2.1. The

numerator corresponds to minus Gibbs free energy variation (-ΔG). Non-spontaneous reactions (electrolytic reactions) have negative values of E^0 and positive values of ΔG, meaning that the higher (in absolute value) the cell potential is the more energy needs to be provided for the reaction to start.

Table 2.1 - Half-cell reactions for each considered product. From it, we calculate the Gibbs energy variation (products - reactants) from tabulated values of the formation enthalpy and entropy. Finally, the cell potential (E^0) is calculated assuming T = 298 K [5].

Product of interest	Anode (oxidation reaction)	Cathode (reduction reaction)	ΔH (kJ·mol^{-1})	ΔS (kJ·mol^{-1})	E^0 (V)
Hydrogen	$2H_2O \rightarrow 4H^+ + 4e^- + O_2$	$4H^+ + 4e^- \rightarrow 2H_2$	572	0.327	-1.23
Carbon Monoxide	$H_2O \rightarrow 2H^+ + 2e^- + \frac{1}{2}O_2$	$CO_2 + 2H^+ + 2e^- \rightleftharpoons CO + H_2O$	283	0.086	-1.34
Methane	$4H_2O \rightarrow 8H^+ + 8e^- + 2O_2$	$CO_2 + 8H^+ + 8e^- \rightleftharpoons CH_4 + 2H_2O$	891	0.243	-1.06

Besides the assembly-based overpotentials, the reaction rate also has influence in the cell potential. Its influence can be described by the Nernst Equation as follows [5], [18]:

$$E = E^0 + \frac{RT}{F \times \log(e) \times n} \times \log\left(\frac{[\text{reductors}]}{[\text{oxidants}]}\right) \quad (7)$$

The concentration of oxidants and reductants can be substituted by their partial pressures since we are dealing with gases.

Another issue that needs to be considered is the type of electrode system of the EC cell. Usually, the EC systems are only analysed in the cathodic half-cell (making the system a 3-electrode cell: anode, cathode which can also be called working electrode and reference electrodes), which is the side where the products of interest are produced (CH_4, CO, H_2), since the anode is always related to H^+ production. This means that the measured potential only belongs to the half-cell and depends on the reference electrode, making it inadequate to introduce in expression (5). Fortunately, the anodic half reaction is always the same (Table 2.1), meaning that the potential difference from half to full reactions is always the same, -1.23 V (that is the hydrogen reaction potential) for the standard hydrogen electrode (SHE) according to [5].

For the purpose of this work, the influence with Temperature also needs to be considered. Although expressions (5) and (6) depend on temperature, they cannot correctly predict changes in temperature for endothermic reactions, because J_0 also depends on temperature, as Vieira explained in his thesis [27]. A better accounting of the temperature dependence has been derived, in which J_0 is expressed as [32], [35]:

$$J_0 = J_0^{ref} \times \exp\left[-\frac{Ea}{R} \times \left(\frac{1}{T} - \frac{1}{T_{ref}}\right)\right] \quad (8)$$

Where Ea is the activation energy (J·mol^{-1}), J_0^{ref} is the current density (mA·cm^{-2}) at the reference temperature T_{ref} (K), T is the working temperature (K). The original equation also includes a factor that

relates the geometrical and active area of contacts, but we have made it equal to 1 as a simplification, since we do not have information about it in the data we have used.

For the calculation of the mass of generated product, the following formula was used [36]:

$$m_i = \frac{s_i M_i I t}{nF} \quad (9)$$

Where m_i is the mass of the specie i that was formed (g), s_i the stoichiometric coefficient of this species, M_i is the molar mass (g·mol^{-1}), I the working current (A) and t the production time (s). The EC efficiency is derived from:

$$\eta_{EC} = \frac{E}{V_{op}} \times E_F \quad (10)$$

Where V_{op} is the operational voltage (V) chosen for the process and E_F the faradaic efficiency which is the selectivity of the process to the desired product.

2.2 Photovoltaic model

The PV systems were simulated based on the single diode model, which corresponds to the following I-V curve [30], [37]–[39]:

$$I = I_{ph} - I_0 \left[\exp\left(\frac{q(V + IR_s)}{\eta_d K_B T} \right) - 1 \right] - \frac{V + IR_s}{R_p} \quad (11)$$

Where I_{ph} is the light generated current (A), I_0 the saturation current (A), η_d the diode ideality factor, q is the electron charge (1.6×10^{-19} C), V the voltage (V), K_B the Boltzman constant (1.38×10^{-23} J·K^{-1}), T the temperature (K), R_s and R_p the series and parallel resistances, respectively.

Since the parameter I_0 is difficult to estimate one can mathematically manipulate expression (11) so that the I-V curve does not explicitly depend from it [38], [39]:

$$I = 1 - (1 - \gamma)^v - \gamma \left(\frac{V^2 + 1}{2} \right)^m \quad (12)$$

$$\gamma = 1 - \frac{V_{oc}}{I_{sc} R_p} \quad (13)$$

$$m = 1 - \frac{1}{\gamma} + \frac{V_{oc}}{N_s n V_T + \theta \gamma I_{sc} R_s} \quad (14)$$

Where $V_{oc}$is the open circuit voltage (V), I_{sc} the short-circuit current (A), R_p the shunt resistance (Ω), V_T the thermal voltage (V), N_s the number of solar cells in series and R_s the series resistance (Ω). θ is an empirical value without any physical meaning.

The PV electric efficiency (EE_{PV}) comes as follows,

$$EE_{PV} = \frac{V_{op} \times I_{op}}{G \times Area} \quad (15)$$

Where G is the solar input power (solar irradiance), usually 1000 $W \cdot m^{-2}$.

2.3 Fischer-Tropsch (FT) model

The FT process consists in the second part of the 2-step process (see Figure 1.1). Here we intend to calculate the energetic cost of this supplementary step, considering temperature change and pressure rise in the calculations. For a constant gas volume, the heat transfer can be represented by the classic calorimetry calculation of heat:

$$Q = m \int C \, dT \quad (16)$$

Where Q is the heat transferred (J), m the mass of gas produced in the EC process that is introduced in the FT chamber (Kg), C is the specific heat ($kJ \cdot Kg^{-1} \cdot K^{-1}$) and T the temperature variation that the gas will suffer, in Kelvin. For our calculations the gas will be heated to 350 °C, since this will ensure that the CH_4 yield is close to 100% for Ni catalysts, according to literature [23].

Considering that the temperature stabilizes and having set the working pressure, the following formula allow the calculation of the energetic cost of pressure (in Joule):

$$E_{A \to B} = P_B V_B \ln\left(\frac{P_A}{P_B}\right) + (P_B + P_A) V_B \quad (17)$$

This formula is obtained from the ideal gas law and E = P×dV. Where P_i and V_i are respectively the pressure (atm) and the volume (m^3) at the instant i. The subscript A stands for the initial condition and B for the conditions at the desired pressure.

3 Results and Discussion

In this chapter all the simulations and results are shown for both the 1-step direct methane production and for the 2-step process with syngas intermediate (see Fig. 1.1).We start by applying the models described in the previous section to both solar and EC cells so we can study them in more detail. Secondly, with the models in place, we are able to simulate different PV-EC systems in order to understand how much, why and how the new state-of-the-art Perovskite/Si solar cells, intermediate electronic regulation (DCDC converter) and the thermal coupling can improve the system's performance. Finally, with these improvements implemented, we conclude about the most energetically efficient path for producing methane, taking in consideration that the 2-step process has an intermediate process, called Fischer-Tropsch that has its own energetic requirements. The results will culminate in the amount (i.e. area) of PV-EC necessary to power an average European house to analyse the feasibility of the concepts and to see if further improvements in the different elements of the system are still necessary.

3.1 Electrochemical reactions

The reactions comprise a complex sequence of steps that unfold after an electric potential is applied. The confirmation that the reaction is occurring is the appearance of an electric current. It confirms that electrons are flowing and that the oxidation and reduction processes are occurring at the respective side of the cell. The higher the current the more gas is produced because it means that more electrons are participating in the redox reactions. In this section we study the J(V) curves of EC cells. Both systems were considered in the same ambient and test conditions, that is, constant CO_2 flux of 20 $mL \cdot min^{-1}$, temperature and pressure at ambient conditions (298 K and 1 atm).

3.1.1 Methane electrolyser (1-step process: $CO_2 \rightarrow$ Methane)

For the methane production (top path in Figure 1.1 which corresponds to Figure 3.1b) we have considered the total cell current from the article Manthiram et al. [8] to model the JV curve. The cathode and anode catalysts are made from Cu and IrO_2 nanoparticles, respectively. Equations (5) to (8) are used in the present model, and the results are shown in Figure 3.1a. The fitting was made in Origin using information from Table 2.1, yielding the fitting parameters indicated in Table 3.1. The starting point are the already known theoretical parameters: *n* assumes the value 8 because the cathodic product is methane which involves eight-electron transfer reactions (Table 2.1); the entropy and enthalpy are the values of methane found in literature and presented in Table 2.1 [5]; the pressure in both sides of the cell is the same (i.e. 1 atm). An ideal flow- through system is assumed in which the gases are always flowing and do not accumulate, keeping their pressures at 1 atm. Only the CO_2 flow is at a slightly higher pressure, 1.2 atm. For simulations at 298 K this is the necessary information, as the missing parameters are inferred using the fitting capabilities of ORIGIN software. However, for

other temperatures we lack information the reaction activation energy (Ea) since the experimental results did not include EC curves at other temperatures.

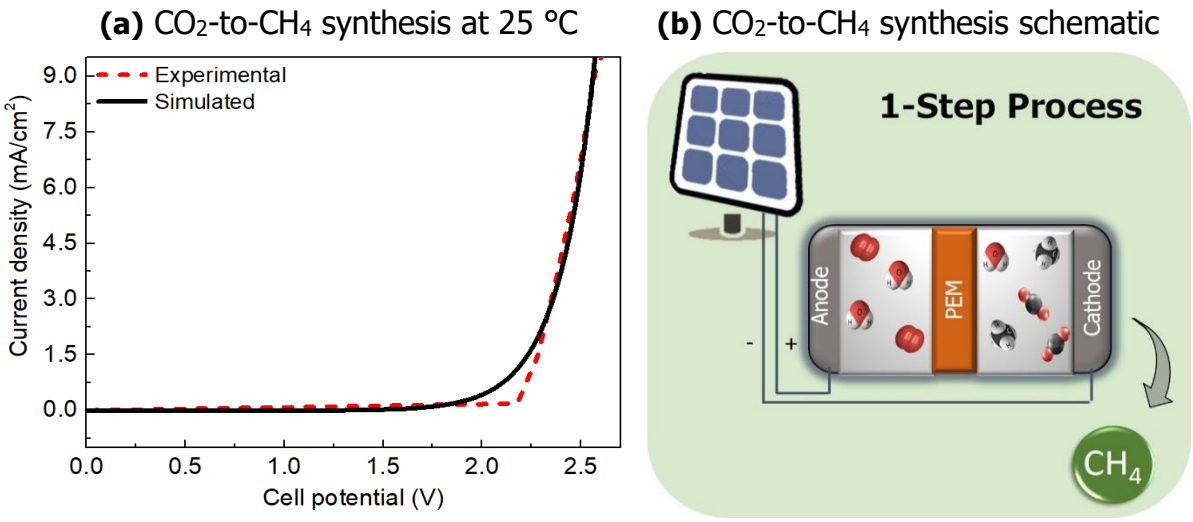

Figure 3.1 – Carbon dioxide to methane EC synthesis: (a) – Experimental [7] and simulated curves at 298 K for the methanation process; (b) - Schematic of the process: connected PV and EC systems to produce methane. Voltage values are presented in absolute value.

Table 3.1 - Parameter set used in the methane electrolyser's model to fit the experimental results.

Fitting Parameter	Value
Ea (J·mol^{-1})	60000
T (K)	298.00
T_{ref} (K)	298.00
J_{ref} (mA·cm^{-2})	0.0162
α_a	0.0000
η (V)	0.1600
α_c	0.1250
ΔH (kJ·mol^{-1})	890.57
ΔS (kJ·mol^{-1})	0.2429
n	8.0000
P_{CH4} (atm)	1.0000
P_{O2} (atm)	1.0000
P_{CO2} (atm)	1.2000

Therefore, the challenging part was the activation energy determination, which is difficult to precisely assess, since it strongly depends on the testing conditions and apparatus. In the literature there are multiple reaction-path models where activation energies can go from 48.3 to 286.6 kJ·mol^{-1} [18]. As a

consequence of not knowing which model fits best this specific experimental data, we have estimated the Ea to be around 60 kJ·mol^{-1} as presented in Table 3.1. Regarding the cell voltage, most works in literature only account for the half-cell potential (i.e. usually measurements only consider the potential between reference electrode and the cathode/working electrode). This is because the reaction of interest is in the cathode side, and the anodic reaction is always the same as can be seen in Table 2.1. However, to properly compare with the 2-step process, we converted this potential to the total potential and in a first simplification neglecting the overpotential of this reaction. Once the anodic half-cell reaction is always the same, as explained in section 2.1, the voltage drop is always -1.23 V (from cathode potential to cell potential the voltage increases 1.23 V in absolute value).

3.1.2 Syngas electrolyser (2-step process: $CO_2 \rightarrow$ Syngas)

The Electrochemical part of the 2-step approach comprises the syngas production (CO and H_2 production in Figure 1.1 which corresponds to Figure 3.2b). The total current data from the article of Kutz et al. [9] was employed to model the JV curves. The paper concerns CO production, however, it is also possible to produce other fuel combinations like syngas. The way we make it possible is explained under section 3.5. The cathode and anode catalysts are made from Ag and IrO_2 nanoparticles, respectively. Equations (5) to (8) are used to model the data, as shown in Figure 3.2.

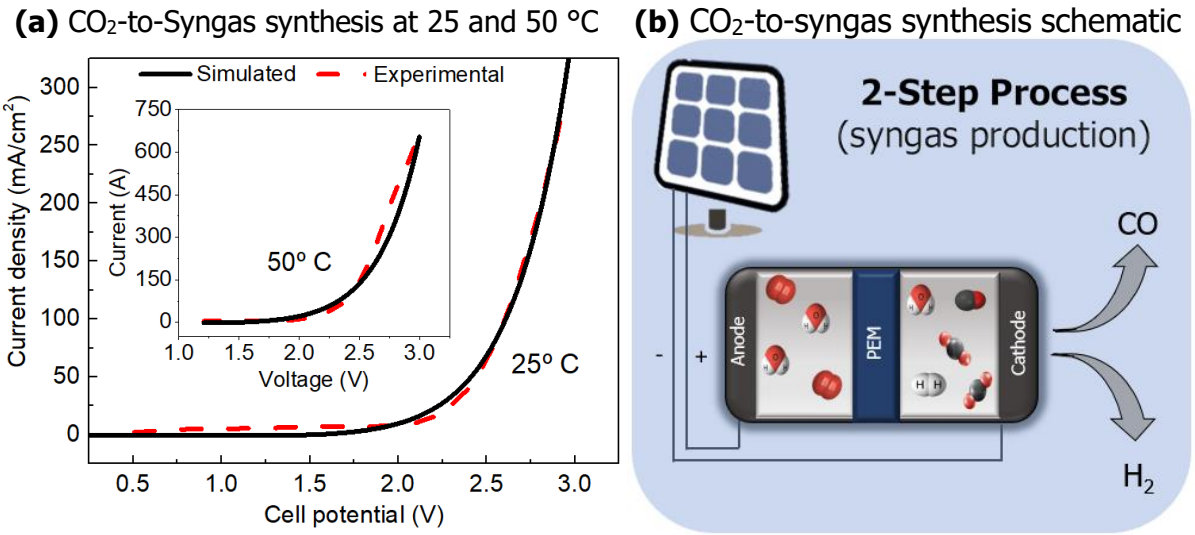

Figure 3.2 –CO_2 to syngas (CO + H_2) synthesis: (a) - Experimental [8] and simulated curves at 298 K and 328 K which show the success of the implemented model at different temperatures; (b) - Schematic of the process: connected PV and EC systems to produce syngas. Voltage values are presented in absolute value.

The fitting was made using information from Table 2.1, yielding the results in Table 3.2. The starting point is the already known theoretical parameter set: *n* assumes the value 2 because both cathodic products –carbon monoxide and hydrogen, constituents of syngas – involve two-electron transfer reactions (Table 2.1); the entropy and enthalpy are the values for carbon monoxide production once this curve was originally for carbon monoxide production. These values can be found in literature and

are presented in Table 2.1 and Table 3.2 [5]; the pressures in both sides of the cell is the same (1 atm). An ideal flow-through system is assumed in which the gases are always flowing and do not accumulate, keeping their pressures at 1 atm. From the first fitting (fitting at 25 °C in Figure 3.2a) we managed to parameterize the anodic and cathodic transfer coefficients ($\alpha_{a,c}$), the overpotentials (η) and the exchange current density (I_{ref}) since the test conditions are the reference conditions (298 K), making equation (8) simply $J_0 \equiv J_0^{ref}$ (removing the influence of Ea). However, Ea is important for simulations at temperatures that vary from the reference one, and it is parameterized at the inset plot of Figure 3.2a. Having data of the same cell at two different temperatures, one can vary the activation energy and see which value provides the best fitting conditions. The most accurate fitting result was 30000 kJ·mol^{-1}. All the model parameters are presented in Table 3.2.

Table 3.2 – Parameter set used in the syngas electrolyser's model to fit the experimental results.

Fitting Parameter	Value
Ea (J·mol^{-1})	30000
T (K)	298.00
T_{ref} (K)	298.00
J_{ref} (mA·cm^{-2})	38.000
α_a	0.0634
η (V)	0.1543
α_c	0.0669
ΔH (kJ·mol^{-1})	283.01
ΔS (kJ·mol^{-1})	0.0866
n	2.0000
P_{CO} (atm)	1.0000
P_{O2} (atm)	1.0000
P_{CO2} (atm)	1.0000

Another evidence that can be extracted from the plots above (Figure 3.1a and Figure 3.2a) is that the two simulations have less accurate fittings at low current densities (below 6 mA·cm^{-2} and 100 mA·cm^{-2} for the methane and syngas electrolysers, respectively). This is due to the Butler-Volmer equation that predicts a smoother (more exponential-like) behaviour when the reaction starts, but the experimental exhibit a more abrupt trend. A deeper study of these cells could mitigate this problem, which we leave for future perspectives.

3.2 Solar cells

The second aspect in the simulation process is to model the PV cells' JV curves. The individual cells and module curves and assembly are represented in Figure 3.3, and their fitting parameters in Table 3.3. The mono-Si curve was simulated according to SUNPOWER's commercially available solar cell, whose datasheet is given in Annex I

. From the datasheet we were able to retrieve the main parameters to our simulation such as the voltage decrease per degree, area, open circuit voltage and short-circuit current at the working conditions of 1000 $W \cdot m^{-2}$, AM 1.5G illumination and 298 K. The remaining parameters of equations (12)-(14) were fitted to match with the experimental JV curve (Figure 3.3a).

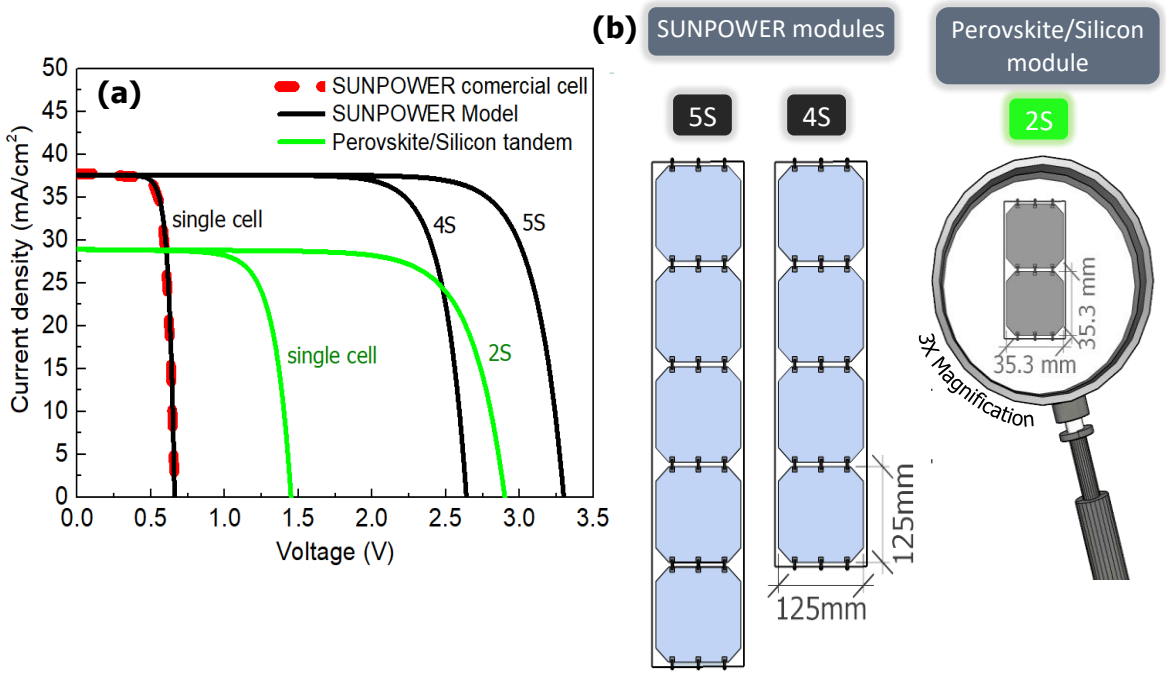

Figure 3.3 – Solar cells considered in the simulations: (a) - Solar cells' JV curves representation at 1000 $W \cdot m^{-2}$, AM 1.5G and 298 K. In green we have the JV curves of a single and 2 series-connected (2S) Perovskite/Silicon tandem cells. The mono-Si arrangements, based on SUNPOWER cells, are represented by the black curves: it shows the JV curves of a single cell and modules of 4 series-connected (4S) and 5 series-connected (5S) cells. Our model for SUNPOWER cell exhibits a perfect fit with its experimental data (in dashed red). SUNPOWER datasheet provided in Appendix I; (b) – sketches of the modules with the different series-connected PV cells, showing their respective size.

In order to analyse an emerging PV technology which can be highly suitable for PV-EC, we considered a Perovskite/Silicon tandem (double-junction) cell with light trapping [10]–[13]. Initial parameters, I_{SC} and V_{OC}, were estimated based on these references. The V_{OC} is in accordance with 2T tandem cell from Hörantner et al. [11], which reaches 1.9 V. With common PV device architectures, current densities close to those of Silicon (i.e. above 30 $mA \cdot cm^{-2}$) are hardly achievable with such high open circuit voltages. However, when considering the implementation of advanced light trapping schemes to boost broadband light absorption (e.g. results from M. Alexandre et al. [13]), and adjusting the cell bandgaps for a lower open-circuit voltage (1.45 V), it is possible to have a cell with a favourable V_{OC} = 1.45 V and

I_{SC} = 30 mA·cm^{-2}. The Fill-factor (FF) and current density of this novel cell design are according to literature, which showed FF up to 83% and I_{SC} close to 30 mA·cm^{-2}.

Table 3.3 – Parameters used in the solar cell model for both mono-Si (SUNPOWER) cell and Perovskite/Si double junction cell. Working conditions of 1000 W·m^{-2}, AM 1.5G illumination and 298 K.

Parameter	Perovskite/Si	mono-Si
Decrease/degree (mV/ºC)	5.800	1.820
Irradiance (W·m^{-2})	1000	1000
V_{OC} @298 K (V)	1.450	0.660
I_{SC} 1000 W·m^{-2} (A)	0.3611	5.870
Rs (Ω)	1.000	1.000
Rp (Ω)	1000	1000
η_d	1.500	1.500
θ	0.4000	0.000
1 cell active area (cm^2)	12.50	156.25

The modules' response was then extrapolated, considering series-connections between individual cells without electric losses. The correspondent quantities of interest are presented in Table 3.4. We have studied two different modules for the mono-Si cells, because we noticed that methane production benefited from having a 5-series cell module (5S), while syngas (CO and H_2 production) benefited from 4-series cells (4S). The FF values are between 72%-79% for the SUNPOWER cell and between 68%-74% for the Perovskite/Si tandem cell. Despite having higher FF values, the mono-Si cells exhibit less than 2/3 in efficiency. Since our tandem cell design is more efficient in converting photons in electricity, we considered a lower active area than that of the SUNPOWER, as we can see by comparing module's sizes in Figure 3.3b. We will see in the next sections which PV type matches best with the EC cells. The analysis of one solar cell technology with high I_{sc} and low V_{op} (mono-Si), and another working with opposite characteristics (Perovskite/Si double-junction), will make an interesting comparison to see which technology is more suitable for EC coupling and to power the subsequent gas fuel production.

Table 3.4 – Representation of the characteristic parameters of the different PV modules studied. The Perovskite/Si double-Junction 2-series cell (2S) module was used to obtain all the products. For Monocrystalline-Si, the 4-series cell (4S) module is used in syngas while the 5 series cell (5S) module is used in methane production only. Solar efficiency is calculated based on the MPP, to be independent of any load.

Characteristic Parameters		Monocrystalline-Si 4S	Monocrystalline-Si 5S	Perovskite/Si Double-Junction 2S
V_{OC} (V)	25 °C	2.64	3.3	2.9
	55 °C	2.58	3.24	2.75
	85 °C	2.53	3.19	2.6
I_{SC} (A)		5.87	5.87	0.36
Fill Factor (%)	25 °C	78.5	78.5	73.8
	55 °C	75.6	75.6	71.3
	85 °C	72.4	72.4	68.4
Solar efficiency (%)	25 °C	19.4	19.4	30.9
	55 °C	17.2	17.2	26.1
	85 °C	15	15.0	21.5
Area (cm^2)		625	781	25

3.3 Photovoltaic-Electrochemical (PV-EC) thermal coupling

In order for the EC cell to receive the maximum possible electric power from the PV, the working point must be close to the solar cell maximum power point (MPP), the reason why the mono-Si and Perovskite/Si double-junction modules have, respectively, 4 and 2 cells in series (Ns parameter in simulations - for the special case of methane production with mono-Si PV, we used 5 cells). This proximity can be depicted between the MPP and the operating point (OP), at 298 K in Figure 3.4. Something also evident in Figure 3.4a is that we lose the proximity to the MPP as the temperature rises, which means that the transfer of power between systems decreases. This is justified by the decrease in PV efficiency while no variation is verified in the EC process, resulting in decreasing current and voltage and, therefore, decreasing output power. A way of mitigating this problem is by **thermally Coupling (TC)** both EC and PV systems, which can be implemented in practise simply by attaching the EC cells to the rear electrodes of the solar cells, as depicted in Fig. 1.2. The improvement can be seen by comparing both plots in Figure 3.4. The thermal coupling allows the EC process to compensate losses (mainly in voltage) in the PV system, because the increasing temperature will positively affect the chemical reactions (evident in the reduction of the EC operating point voltage with constant operating current). While in the uncoupled system (Figure 3.4a) the operating current density reduces from 33 $mA \cdot cm^{-2}$ to 15 $mA \cdot cm^{-2}$ when heating from 25 to 85 °C, the coupled system (Figure 3.4b) manages to stabilize the output current around 33 $mA \cdot cm^{-2}$. This will have major influence in improving

the system's efficiency and consequently gas production. Other ways of approximating even further the operating point to the maximum point will be discussed in the following chapters.

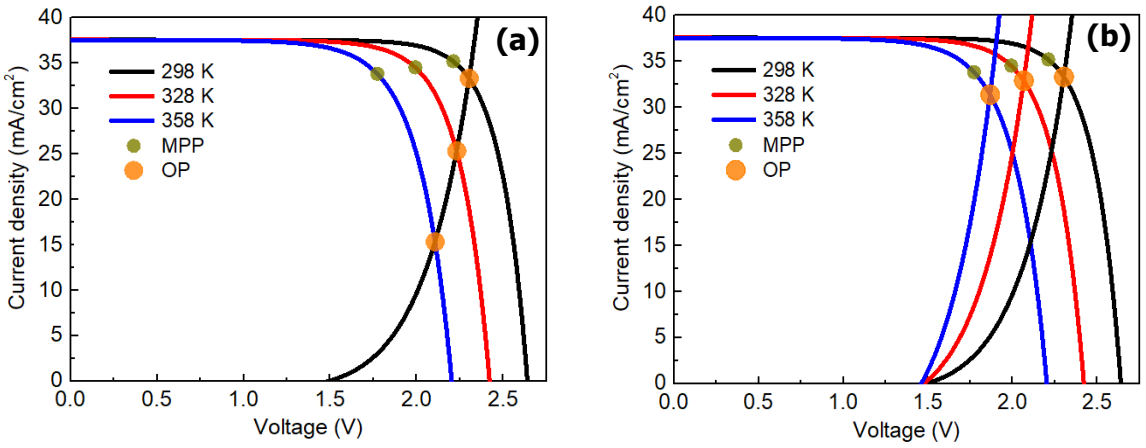

Figure 3.4 - Simulation of the PV (i.e. Si) and EC (i.e. syngas electrolyser) systems for 3 different temperatures: 298 K, 328 K, 358 K: (a) – is the uncoupled system; (b) – is the thermally coupled system. The solar maximum power points (MPP) and operating points (OP) are represented at each curve. We represented a Si-syngas system, but the others operate accordingly.

3.4 Process efficiency

After modulating the individual systems, it is time to test how the systems combine with each other and how much influence can thermal coupling have. We can evaluate this based on the process efficiency. To calculate the process efficiency, we need the solar-to-electricity efficiency (EE_{PV}) and the electrochemical efficiency (EE). From a solar irradiance of 1000 $W \cdot m^{-2}$, the solar panel area and the operating point (obtained from the JV plots like the one in Figure 3.4), one can use Equation (15) to compute the EE_{PV} (Figure 3.5b). The results show that if the system is thermally coupled (TC), the Perovskite/Si double-junction cells are more efficient because the modules' efficiency varies from 22% to 30% while the mono-Si vary from 12% to 20%. The specific case of the 1-step process without thermal coupling (NoTC) powered by Perovskite/Si double-junction cells (1-step, NoTC + Perovskite/Si – green curve with green squares) show that NoTC can drastically change the PV efficiency and consequently degrade the system's performance. Despite this specific case, where above 50 ºC the mono-Si modules are better, Perovskite/Si cells show higher potential.

The EE (Figure 3.5a) comes from equation (10) which depends on the operating voltage and faradaic efficiency. The latter is taken to be 80% for CH_4 [40] and 96.7% for the syngas electrolyser [9]. In future considerations we will assume the same value of 96.7% for H_2 synthesis, since we know from literature that hydrogen can be produced with high selectivity, sometimes even considered 100% [32], [33]. Once the two products (CO and H_2) have the same selectivity, the EE will be the same for the different product ratios. The electrochemical energy efficiencies for these electrolysers

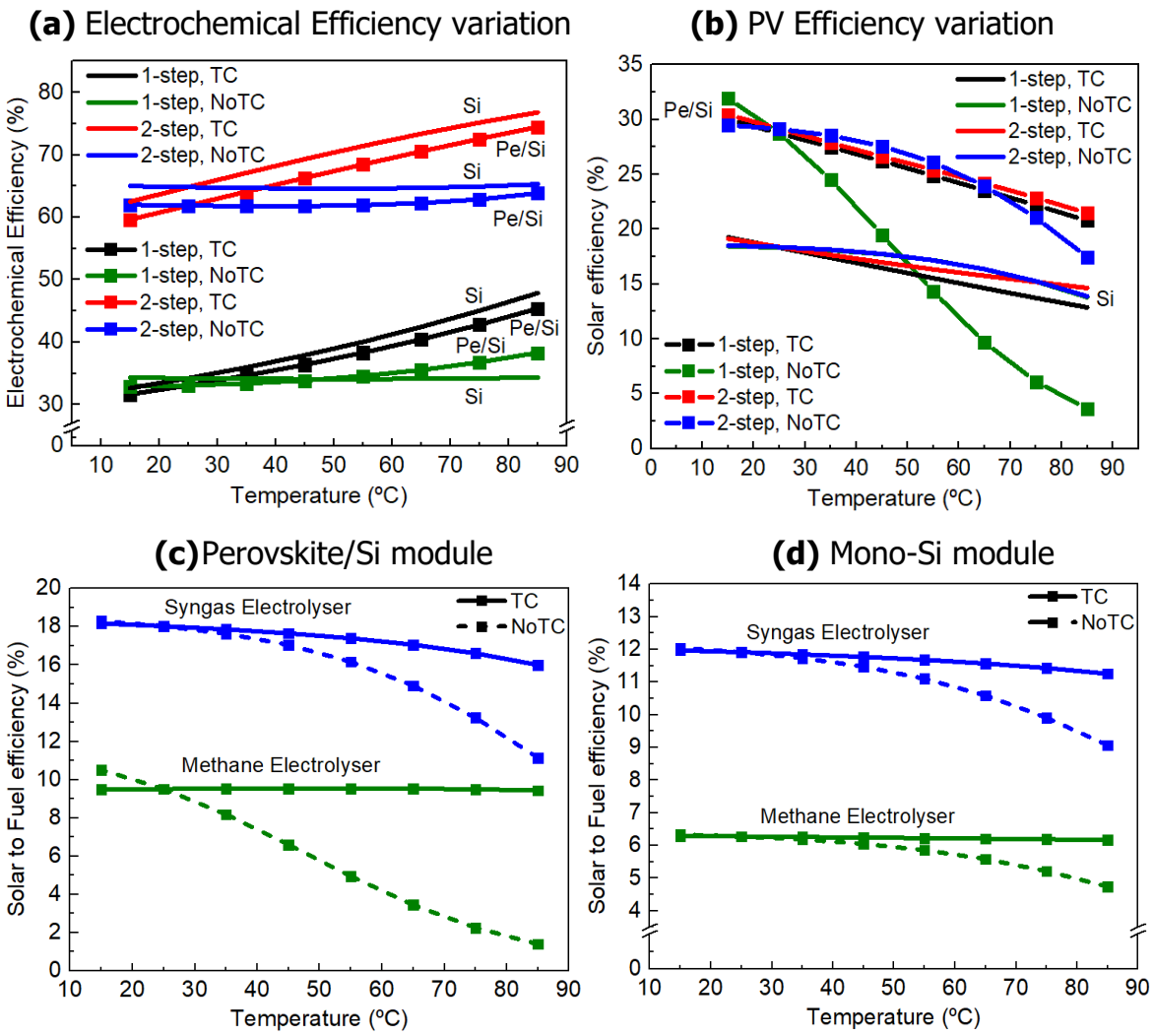

Figure 3.5 – Solar-to-fuel efficiencies of the studied electrolysers : Plots (a) and (b) show the EC and PV efficiency, respectively, for the two electrolysers in combination with the two types of PV (mono-Si and Perovskite/Si). Plots (c) and (d) show the overarching solar-to-fuel efficiency - the curves in blue correspond to the CO_2-to-syngas electrolyser, which will be responsible to produce multiple CO:H2 ratios depending on the cathode constitution, and the curves in green correspond to the CO_2-to-methane electrolyser. A comparison between Thermally Coupled (TC) and Thermally Uncoupled (NoTC) systems is made, where the uncoupled systems show decreasing efficiency with increasing temperature. Plots (c) and (d) differ in the type of solar cells used. In (c) we tested a module of 2 Perovskite/Si tandem (double junction) cells connected in series while in (d) we used a module of 4 (for syngas) or 5 (for methane) monocrystalline Silicon cells from SUNPOWER connected in series.

are placed between 30% and 80% (1.5x to 2x higher for the 2-step electrolyser) which tend to increase with temperature. It is possible to conclude that the syngas electrolyser (in 2-step route) is more efficient than the direct methane electrolyser (1-step route). In general, the Perovskite/Si modules have lower electrochemical efficiencies than the SUNPOWER cells modules, but higher PV efficiencies. The PV efficiency difference is higher, so the Perovskite/Si module provides higher solar-to-fuel efficiencies ($EE_{PV} \times EE$, presented in Figure 3.5c,d). In each figure (Figure 3.5c and d) we confirm that the methane electrolyser has lower efficiency than the syngas electrolyser. Also, by comparing both figures, we see higher efficiencies for the Perovskite/Si modules. It is also possible to identify great differences between the Coupled (TC) and uncoupled (NoTC – dashed lines) systems. What usually happens is that the EC

compensates the PV when temperatures increases: In normal conditions (NoTC) only the PV needs to be under direct sunlight, which means that it is the only system that will to heat up, hence its efficiency will decrease during solar exposure (Figure 3.5b). On the other hand, when we couple the EC system (TC conditions) we allow thermal equilibrium between both systems which means that both will get warm. The PV will still reduce efficiency, however, a higher temperature EC system allows efficiency improvements (Figure 3.5a) because reaction kinetics are favoured. Consequently, the TC curves will have small to no degradation with increasing temperature since the EC system's efficiency improvements compensate the efficiency decrease of the PV system. TC will be beneficial to the process (i.e. improves the solar-to-fuel efficiency) until up to 576% and 30% for the Perovskite/Si double-junction and Si solar modules, respectively, in comparison to the system without it. The 576% has to do with the specific combination of the methane electrolyser and the Perovskite/Si double-junction modules. From 15 °C to 85 °C the operating current changes drastically, which lowers abruptly the EE_{PV} and consequently the solar-to-fuel efficiency. This shows a limitation of cells with high open circuit voltages (which is the case of Perovskite/Si double-junction with V_{oc} = 1.45) when used with uncoupled systems: it is difficult to adjust the operating point by adding individual series-connected cells, because it would be 1.45 V away from the previous one, which despite being able to increase the operating current, it would place the operating point further away from the MPP, which would lead to a great amount of power lost.

3.5 Fuel production

In this work we are studying two different electrolysers that can output either methane or syngas (carbon monoxide, CO, and hydrogen, H_2). For the syngas electrolyser (2-step) a greater challenge is proposed, because we want to produce two gases at the same time with specific relative concentrations. Usually EC systems concentrate production in one gas, while the remaining are unwanted by-products. Here we could also produce CO and H_2 in separate electrolysers, however, it would require a bigger infrastructure to deal with two separate EC systems. Instead, we consider the system of Masel et al. [19] in which the composition of the cathodic products can be manipulated to tune the CO:H2 ratio. In other words, while keeping the same EC behaviour (JV curve) we can manipulate the cathode composition between a metal with more affinity to CO (e.g. Ag) and a metal with more affinity to H_2 (e.g. Ni), to choose the desired proportion of gases at the output. For example, at the same operating point, an Ag:Ni ratio of 1:2 gives an output CO:H_2 ratio of around 1:1. At this ratio the proportion is quite stable independently of small changes in the operating point. For higher ratios the stability of the gas ratio gets closer to the metal's ratio (i.e. Ag:Ni ratio of 1:4 gives CO:H_2 ratio of 1:4), but small operating point changes can easily alter the output ratio of gases. Anyway, this system has proven that an EC cell, initially designed for carbon monoxide production with >95% efficiency, can also produce other fuels just by changing the cathode composition. We will make use of this property so we can model syngas production with different CO:H_2 ratios (1:0, 1:1, 1:3, 0:1). The studied paper reference

only refers a two-metal cathode from 2 different output gases, but probably it might accommodate more complex product combinations for more complex productions: this is an aspect that can be further studied in the future.

For fuel production estimation one need to calculate the mass of gas produced which depends on the operating current - Equation (9). The results for the produced mass are present in Figure 3.6.

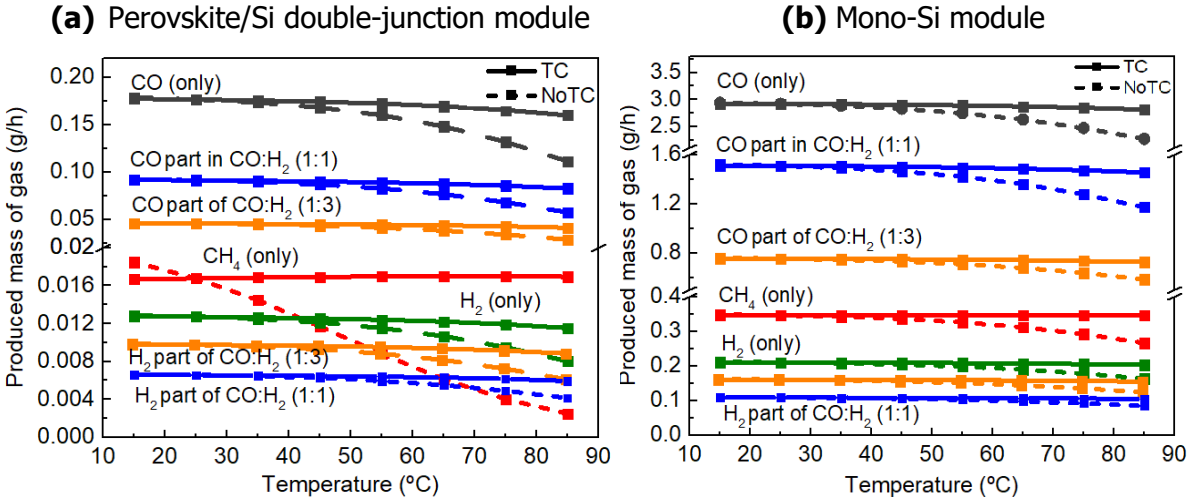

Figure 3.6 – Total mass of gas fuel produced from both electrolysers. Multiple CO:H2 ratios were simulated. Results of both thermal coupled (TC) and uncoupled (NoTC) systems are presented. Each colour represents a different apparatus of EC cell to output the desired gas. A Faradaic efficiency of 96.7% is taken for the syngas electrolyser [9], while for CH4 we assumes 80% [40].

The produced mass flow (g/h) of fuel is what matters the most in a system like this, however, it must not be evaluated without considering also the efficiencies presented in Figure 3.5. The amount of gas produced is given by the current: the higher the current the higher the mass of fuel produced, as Equation (9) states. This could easily be accomplished with bigger PV modules (more series connections or larger cells). However, this does not mean that we are creating the best system for this purpose, especially if we have space limitations at the time of implementing the system. With this we would be wasting power that the PV could provide to the EC system. These thoughts help us to compare the two systems. We found that the PV-EC with Perovskite/Si double-junction cells module is more efficient, while the mass production per hour is higher for the mono-Si single-junction cell. The operating voltage is around the same values for both solar panels which makes the EC efficiency identical. However, while the Perovskite/Si tandem reaches the operating point value with only 2-series connected cells (each cell V_{OC} = 1.45 V), the mono-Si solar cell needs 4 or 5 (each cell V_{OC} = 0.66 V), greatly increasing the area and, therefore, reducing the PV efficiency and consequently the total solar-to-fuel efficiency. On the other hand, mono-Si panels have higher operating currents (around 36 $mA{\cdot}cm^{-2}$ while Perovskite/Si has around 27 $mA{\cdot}cm^{-2}$) meaning the mass of produced gas will be higher because its production is directly related with the number of electrons created - Equation (9). For a fair comparison we created a metric for the production: production-over-area ratio (POAR) in $L{\cdot}h^{-1}{\cdot}m^{-2}$. It relates the production of

wanted gas (in Liters) with the working time and PV area. Here we can see that the Perovskite/Si technology can achieve better results (Table 3.5).

Table 3.5 – Production over area ratio (POAR) for the two production mechanisms at the different PV conditions. Results are given for three different PV temperatures: 25 °C, 55 °C, 85 °C. The syngas values show the results for independent production of CO and H_2 (which have the same rate, since the cathode selectivity is about the same) and for simultaneous production of CO and H2 at the proportion of 1:3.

		Production-over-area ratio ($L \cdot h^{-1} \cdot m^{-2}$)			
		Perovskite/Si Double-Junction		Monocrystalline-Si	
		Thermal-Coupled	Not TC	Thermal Coupled	Not TC
CH_4	25 °C	10.2	10.2	6.75	6.75
	55 °C	11.4	5.91	7.44	7.00
	85 °C	12.4	1.84	8.12	6.24
CO or H_2	25 °C	61.7	61.7	40.8	40.8
	55 °C	66.2	61.5	44.4	42.2
	85 °C	67.1	46.8	47.2	38.1
CO in $CO:H_2$ (1:3)	25 °C	16.0	16.0	10.5	8.60
	55 °C	17.1	15.9	11.5	9.36
	85 °C	17.4	12.1	12.2	9.97
H_2 in $CO:H_2$ (1:3)	25 °C	47.8	47.8	31.6	25.7
	55 °C	51.3	47.7	34.5	28.1
	85 °C	52.1	36.3	36.6	29.9

The volume of produced gas will be dependent on the mass value calculated in Figure 3.6 and temperature. If the mass is stable (usually in TC system) the volume tends to increase as the temperature increases (ideal gas law). This is the reason why, in Table 3.5, Syngas with TC has higher rates for high temperatures. This does not happen with NoTC systems because the mass of gas produced reduces with temperature increase. In this table we also show the independent ratios of CO and H_2 in the syngas production. Despite our main interest being $CO:H_2$ at a ratio of 1:3, we provide in Table 3.5 the POAR of different production ration to emphasise the versatility of such system. From analysing the table, it becomes evident that the PV-EC system using Perovskite/Si Double-Junction cells module is better and that the combination with the syngas electrolyser gives the best results.

3.6 Intermediate electronic regulation

As seen in the previous section, the Thermal coupling has manifested as an important mechanism to stabilize the operating point and consequently improving the gas yield for the different working temperatures. However, other varying parameters such as solar intensity will also have influence in the

system's performance. For this, complementary mechanisms such as intermediate electronic regulation between the PV and EC can further increase the system's stability and rate of production. Using an active DC-to-DC (DCDC) converter between the PV and EC will be important not only for operating point stabilization, since the sunlight instabilities affect the operating point and harm the EC cell, but also to make use of all the power that the PV can supply. In particular, state-of-the-art switched-mode DC-to-DC converters have shown high energy efficiencies (up to ~98%) due to the use of power FETs which are able to switch quite efficiently with low switching losses at high frequencies (e.g. as compared with bipolar transistors), thereby enabling fast semiconductor device rise and fall times that also reduce the heat-sinking need. Besides, the use of synchronous rectification with power FETs provides very low "on resistance", thus reduced switching losses [41]. Therefore, in order to simplify the analyses of PV-EC solutions as those performed in this work, the power efficiency of state-of-the-art DC-to-DC converters can be considered approximately ideal, due to their extremely low electric losses relative to those of the other system components.

In this study we tested the use of a DCDC converter as explained in Figure 3.7. In Figure 3.7a the dashed curve represents the line in the plot where the power is the same as that provided by the PV (i.e. in the MPP). Assuming 100% DCDC converter efficiency the operating point can go from (2.1 V;15 $mA{\cdot}cm^{-2}$) to (2.2 V; 27 $mA{\cdot}cm^{-2}$). This is particularly interesting for the cases where the biggest gain is in current not in voltage (for this example, there is 80% gain in current while voltage only increases 5%). High boost in voltage would lead to improved PV efficiency but decrease in EC efficiency, while increase in current favours both PV efficiency and produced mass of gas. Also, the solar-to-fuel efficiency (equations (10) and (15)) will only depend on the current, not on voltage. Therefore, DCDC improvements are higher if we are working with a steep (the more vertical the better) EC curve, because the MPP power available is used in increasing current and not voltage.

The results obtained are shown in Figure 3.7b, for both SUNPOWER (right side) and Perovskite/Si tandem (left side) solar modules. We have tested for 50 °C, since this is an adequate average temperature expected in roof-mounted PV installations [42] (as sketched in Figure 1.2). According to this work, even outdoor temperatures below 30 °C can easily translate into 50 °C for sun-exposed PV systems placed on the rooftops. In Figure 3.7b the improved percentage is equal to both the solar-to-fuel efficiency and the mass of gas produced, due to the increase in current (voltage is not represented in both equations). The data without percentage increase means that no significant improvement was verified for that specific temperature. Excluding the best result of 50% gain relatively to a system without DCDC, the results were more modest than we expected, always below 10%. However, it is not a disappointing result because we have proven that DCDC converters can be more useful than just for stabilizing the operating point. Also, at every temperature the DCDC converter results are different. Appendix I and II show all the combinations and the comparison in solar-to-fuel efficiency and mass (represented by the POAR – which is proportional to the produced mass), respectively, of the system with and without the DCDC converter. Depending on the temperature there might be room for

improvement or not. Regarding solar-to-fuel efficiency the improvements are higher for the lowest and highest temperatures (15 °C and 85 °C) while the mass or POAR results are more inconsistent.

For a better understanding of the improvements attained with TC and DCDC regulation, we created Table 3.6. Here, we can see how the POAR is affected by these effects. For ambient and low

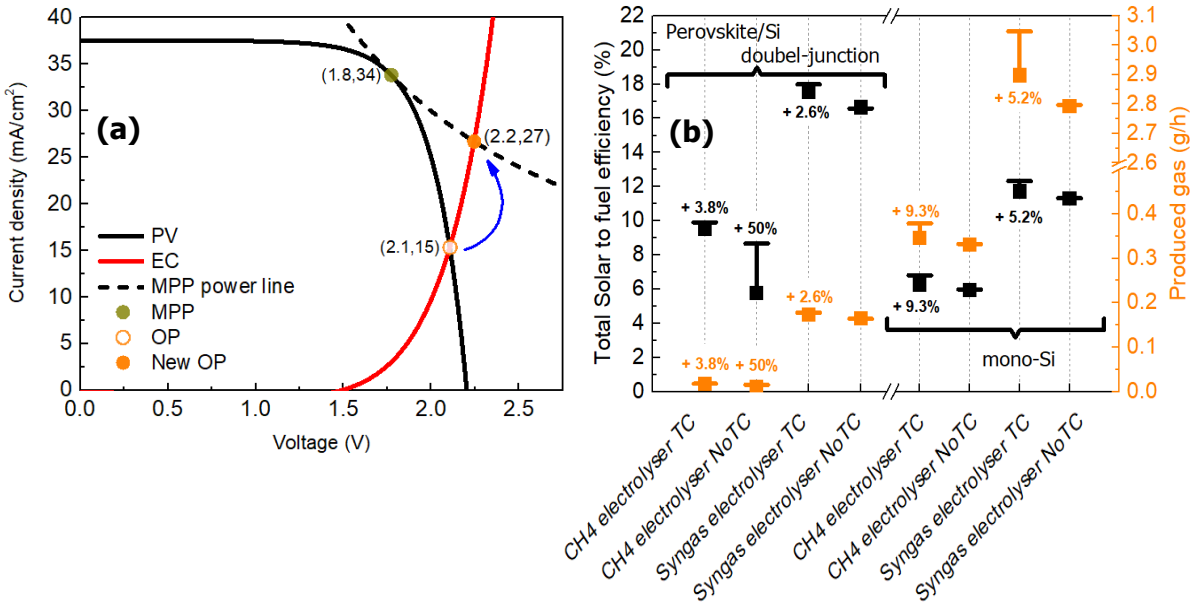

Figure 3.7 – Results of the use of a DCDC converter between PV and EC for 50 ºC: (a) - Methodology used for DCDC converter tests/simulations. By identifying the maximum power point (MPP) of the PV we can trace the equivalent power line (dashed black) and find a better Operating Point (OP); (b) - mass and solar-to-fuel efficiency with and without the DCDC converter for the mono-Si and Perovskite/Si cell, respectively. The values at each point represent the improvement (in percentage) allowed by the DCDC converter. The points without number did not have significant improvements.

temperatures (close to 25 °C) the thermal coupling has low to no influence, meaning that only the DCDC converter can assist production, with improvements around 5% for both solar modules. For higher temperatures the influence of thermal coupling becomes more evident, boosting production of a system without both DCDC and TC up to 586% and 42.9% for the Perovskite/Si double-junction and mono-Si solar modules, respectively. As seen in Figure 3.7b some uncoupled systems have no improvements in using DCDC converter. However, when conjugated with thermal coupling the DCDC converter often boosts production, with improvements that can go up to 14%, besides the already existing TC improvement.

The DCDC improvements for one temperature could also be achieved by tuning the area proportion between the PV and EC. Here we have studied equal areas since it is simpler to assemble and produce (see Figure 1.2). However, if we reduce the EC area relatively to that of the PV, we can lower every operating point voltage that is higher than the MPP voltage and match it with the MPP. It would be challenging to perfectly match considering all production variables. Also, this would only allow a perfect match at one temperature, so a DCDC converter would still be necessary for the rest.

Table 3.6 – Production-over-area ratio (POAR) using DCDC converter and its gain (in %) compared with the system with only thermal coupling (without DCDC) and the system without both thermal coupling and DCDC. Results are given for both types of electrolysers.

		Production-over-area ratio using DCDC converter ($L \cdot h^{-1} \cdot m^{-2}$)					
		Perovskite/Si Double-Junction			Monocrystalline-Si		
Electrolyser		Thermal Coupled & DCDC	Gain vs TC without DCDC (%)	Gain vs NoTC without DCDC (%)	Thermal Coupled & DCDC	Gain vs TC without DCDC (%)	Gain vs NoTC without DCDC (%)
CH_4	25 °C	10.8	5.40	5.40	7.11	5.31	5.31
	55 °C	11.7	2.81	98.1	8.13	0.00	16.2
	85 °C	12.6	1.55	586	9.26	14.1	48.4
syngas	25 °C	64.9	5.20	5.20	42.8	4.87	4.87
	55 °C	68.0	2.72	10.5	46.4	4.53	10.0
	85 °C	66.8	0.00	42.9	47.9	1.52	26.0

3.7 Fischer-Tropsch synthesis (FTS) and energetic comparison of processes

For a fair comparison between the two steps of Figure 1.1 we calculated the energetic output of both paths (i.e. for the 1-step and 2-step that culminate with CH_4 production).

At first, a simple analysis can be made considering the two processes and heat values of the products. When we go all the way through step-2 and convert syngas into methane, we start with 4 moles of gas with heat value of 1000 $kJ \cdot mol^{-1}$ (1 mole of CO of value of 283 $kJ \cdot mol^{-1}$ and 3 moles of H_2 of 240 $kJ \cdot mol^{-1}$) and only obtain one mole of CH_4 worth 800 $kJ \cdot mol^{-1}$, as equation (4) states, which is the same end result of the 1-step process (1 mol of CH_4 worth 800 $kJ \cdot mol^{-1}$). If we ignore FTS losses, the 2-step process would be preferable because it has the same heat value as the 1-step and higher solar to methane allowing higher production of energy (pink curve vs black curve in Figure 3.8). Even better would be the 2-step without FTS if we could use syngas the same way as we use methane. The 4 moles of $CO+H_2$ and the higher process efficiency achieve up to 1.6 times more power compared with the 1-step process. However, infrastructures are implemented for methane, so we need to consider the FTS and its losses. These energy losses will be decisive in the choice of which process is the most energetically rentable. Calculations for deciding the best path for methane production are given below.

For power conversion the lower/net calorific/heating value (LHV) of CH_4 was used, which is 35.8 $MJ \cdot m^{-3}$ (9.9 $kWh \cdot m^{-3}$) [43]. The methods will be compared based on the amount of energy the process can produce by unit area of PV ($W \cdot m_{PV}^{-2}$). This can be obtained by conjugating both the LHV of CH_4 with the PV-EV production ratio presented in Table 3.6.

Considering a temperature of 298 K, the 1-step results are straightforward: 107 $W \cdot m_{PV}^{-2}$ and 70.4 $W \cdot m_{PV}^{-2}$ for, respectively, Perovskite/Si double-junction and mono-Si PV cells.

For the 2-step process we not only need to consider PV-EC system, but also the FTS process to convert syngas to CH_4 (as Figure 1.1 shows). At the output of the EC system we have CO and H_2, both with individual energetic values. By considering 10.8 $MJ \cdot m^{-3}$ for H_2 and 10.1 $MJ \cdot m^{-3}$ for CO [43], one has a total energetic capability of 195 $W \cdot m_{PV}^{-2}$ and 128 $W \cdot m_{PV}^{-2}$ for the Perovskite/Si double-junction and mono-Si PV cells, accordingly. The POAR for H_2 is 3/4 (1/4 for CO) of the POAR for syngas electrolyser in Table 3.6. At a first glance we see that this yields an 80% higher (i.e. close to 2x) energetic value than the direct production of CH_4. However, syngas is not the product of interest and we still need to account for the losses present in the FTS conversion. The results are presented in Figure 3.8. For the FTS process we have considered a lossless conversion chamber where the main energetic requirements are those necessary to achieve the working Temperature and Pressure, which are 350 °C and 10 to 30 atm, respectively. We have chosen this working condition from literature: According to Gao et al. [23], despite low temperature favouring the reaction from the thermodynamic point of view, the catalysts are not active below 350 °C and we need them working to avoid production of unwanted side-products. Since this Temperature is an interesting working point from the efficiency point of view (CH_4 yield >99%), it was chosen. Higher temperatures will also introduce other process problems, if combined with low pressure (below 15 atm), like carbon deposition on the catalysts which would lead to reducing the selectivity of the process. Regarding pressure, if it is too low (below 10 atm) the yield is below 95%. Above 10 atm, costs are higher, but the reaction is favoured since it is a volume reducing reaction. Above 30 atm no major advantages are verified below 700 °C. We will assume a 30 atm pressure as starting point and will compare the results with a 10 atm process. Gao et al. performed a thermodynamic analysis which, for the chosen conditions, complies very well with two commercial nickel-based catalysts (N112, NiO 67 wt%, JGC Catalyst and Chemicals Ltd., Japan and HT-1, NiO 57 wt%, LiaoNing HaiTai SCI-TECH Development CO., LTD, China).

To determine the energetic cost of temperature increase we used equation (16). The information regarding the specific heat variation with temperature was taken from literature [44], [45]. Despite depending on temperature, the specific heat is considered constant for processes with small temperature changes. However, this process deals with a temperature change of 325 °C (from 25 °C to 350 °C), meaning that this influence cannot be discarded. The mass was calculated based on the results presented in Table 3.5 and considering the initial conditions of the chamber to be 1 atm and 298 K. The requirements of the two reagents (CO and H_2) were calculated separately and added at the end, giving a need of 6.8 $W \cdot m_{PV}^{-2}$ and 4.55 $W \cdot m_{PV}^{-2}$ for the Perovskite/Si and mono-Si cells, respectively. The value for the mono-Si is smaller because its production rate is inferior. Both reagents require around the same amount of heat (3.2 $kWh \cdot m^{-3}$ for CO and 3 $kWh \cdot m^{-3}$ for H_2), however, since we have three times more hydrogen than carbon monoxide, the heat required for H_2 will be roughly 3 times higher.

For the Pressure rise calculations we apply Equation (17). Considering an initial pressure of 1 atm (output of EC cell) and final pressure of 30 atm we obtain a total cost of 1.96 $kWh \cdot m^{-3}$ (0.33 $kWh \cdot m^{-3}$ for 10 atm). By computing this with the corresponding rate of production at which the reaction occurred (from Table 3.6 at 298 K), one obtains the values of 132 $W \cdot m^{-2}$ (23 $W \cdot m^{-2}$ at 10 atm) for Perovskite/Si double-junction and 83.9 $W \cdot m^{-2}$ (15.4 $W \cdot m^{-2}$ at 10 atm) for mono-Si. By comparing the cost of pressure (light-pink for 30 atm and middle-tone-pink for 10 atm) with the cost of temperature (dark-pink area in Figure 3.8) we see that the pressure has more weight in the total energetic cost. Therefore, it becomes a determining factor for the 2-step process to get more energetically advantageous compared with the 1-step. For a process at 30 atm (light-pink area in Figure 3.8) the net energetic value of the process (value of the fuel products minus the cost of the process) falls below the energy of the 1-step process. The 2-step is only preferable at a pressure close to 10 atm (mid tone pink area in Figure 3.8). In this condition the 2-step process has 20% and 23% more energetic potential than the 1-step, for the Perovskite/Si double-junction and mono-Si PV modules, respectively.

In Figure 3.8 we have all the previous results represented according to the daily sun hours for each

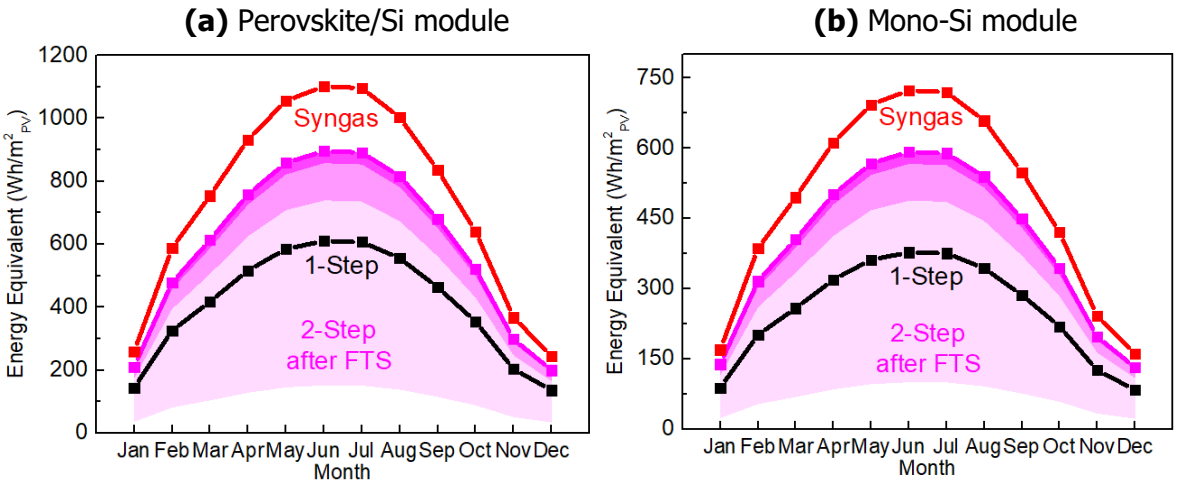

Figure 3.8 – Annual fuel energy equivalent production powered by Perovskite/Si cells, (a), and mono-Si cells, (b). The red curve shows the energetic capability of syngas in the 2-step process, after the EC stage. The pink part with three tonalities corresponds to the complete 2-step process, where the curve is the energy harvested in methane form, after the FTS process, and the pink filled areas represent the FTS process losses to obtain methane: the darkest part right below the curve is the energetic cost to increase temperature while the rest (the main cost) comes from pressure increase, being the middle pink region for 10 atm and the lighter region for 30 atm. Everything considered, the 2-step final energy (in methane) at 30 atm is lower than the 1-step process (curve in black).

month. These plots consider a yearly average of 4 peak sun hours per day for Europe. The peak sun hours correspond to the conversion of the number of hours in a day, with variable solar intensity, into solar hours at an irradiance of 1000 $W \cdot m^{-2}$. The results show higher produced energy for the summertime when there are more sun hours per day. The higher production rates reveal that the Perovskite/Si modules are better energy producers than the mono-Si ones. At a first glance the 2-step process seems to have higher energetic output, as we have seen before when we compared the direct methanation EC process with the syngas production. However, if the downstream FTS process is run at high pressure (above ~15 atm), and is not powered by solar energy or any other green energy

method, the high energetic costs for the process makes it less attractive. However, if we work at 10 atm it is possible to output more power from the 2-step process than from 1-step process.

3.8 Building integration study

In this section we estimate the size of a PV-EC system required to power an average household. With the information from the previous section we know how much energy a system like this can produce. Therefore, we can compare it with how much a typical household consumes, in order to identify the necessary size of such implementation. Considering the primary energy consumption for an European household of 11630 kWh per year [27], [46], we estimate that to satisfy the demand, we would require 55 m^2 and 81 m^2 of PV-EC system for the 2-step route (83 m^2 and 123 m^2 for 1-step) for, respectively, the Perovskite/Si and mono-Si modules. These calculations were made considering the annual integration of the curve in Figure 3.8 (pink curve for 2-step and black curve for 1-step). These results are only possible if there is a way to store excess fuel/energy from the months when production is higher (Summertime) to satisfy the demand in other periods. If this is not possible, we have also calculated the area for the worst-case scenario, which is considering the production of every month to be the production of the worst month, December. The results show that it is necessary 160 m^2 and 237 m^2 of PV-EC system for 2-step (242 m^2 and 360 m^2 for 1-step) for, respectively, the Perovskite/Si and mono-Si cells. It is more than 3x the first approach with storage.

To understand if these systems are feasible to implement, we must find which is the average roof area for an European household. If we consider the results of Salvador Izquierdo et al. [47] regarding the Spanish (as an European representative case) roof area per capita of 14 ± 4.5 m^2/ca., and the average European household of 2.25 persons [48], we can estimate that an average European household has a rooftop area of around 31.5 ± 10.1 m^2. This result shows that it will be difficult to implement such system entirely on the roof because the PV-EC system requires, at least, 55 m^2: facades or backyard exposed to the sun must be used. This means that improvements have still to be made both in reducing energy consumption in buildings (e.g. with energy-efficient architectures and combination with solar thermal) and in the development of PV and EC technology in order to make the systems even more compact (with higher power density), in view of future net-zero energy buildings fully solar-powered.

4 Conclusions

For the purpose of this work we performed the simulation of two solar-powered electrochemical systems, where the main goal is to study how different synergetic solutions, namely the use of thermal coupling and intermediate electronic regulation, can positively influence the performance of PV-EC systems. Throughout the entire work the cells were assumed to be in a compact PV-EC system, where solar panels provide the necessary power for the reactions to occur. Two methane production paths were chosen in combination with two different sets of solar cell technologies. The referred performance boosters were implemented to these systems in order to understand its importance and anticipate the most energetically efficient path, and how viable it can be to have an environmentally friendly carbon-based fuel system like this at our home.

The direct methane production, 1-step process, has low selectivity (80%) which leads to low efficiency. Therefore, we compared it with a more complex pathway for obtaining methane, the 2-step process, that obtains methane through an intermediate compound, syngas, by a conversion reaction, the Fischer-Tropsch process. In terms of solar panels, we compared a well-established and commercial technology, SUNPOWER mono-Si solar cells, with state-of-the-art Perovskite/Silicon tandem cells.

Results show that thermal coupling is always beneficial to the process stability because the improvement in the reaction kinetics with increasing temperatures allows for the solar-to-fuel efficiency to be up to 576% relative to uncoupled systems for Perovskite/Si double-junction cells (up to 30% for SUNPOWER cells). On the other hand, when not using any thermal coupling nor electronic regulation, solar cells with high open-circuit voltages like the Perovskite/Si double-junction (Vop = 1.45 V) are worst because the operating point will easily miss the PV's MPP (difficult to adjust with series connections because the voltage unit is always 1.45 V), which makes them more vulnerable to temperature changes. Regarding the intermediate electronic regulation (DCDC) we showed that it can also contribute to the improvement in production, despite the more modest results: improvements can go up to 50% in solar-to-fuel efficiency or mass of gas produced for the Perovskite/Si double-junction. We noticed that the steeper the EC curve close to our operating point (i.e. initial operating point just by combining the PV and EC – operating point before DCDC adjustment), the better the DCDC improvements will be, because when the new operating point is defined with the aid of the DCDC converter, so the power usage gets closer to that of the PV MPP, there is more room for increasing current than voltage, leading to higher amount of gas produced.

From the point of view of PV-EC yield, syngas production with Perovskite/Silicon tandem cells showed to be the most solar-to-fuel efficient, with 18% efficiency at room temperature against 12% for SUNPOWER cells. Despite the higher current density for the mono-Si cell, which could suggest more fuel production, due to small open-circuit voltage of (0.66 V), it requires twice or more series connections (i.e. higher panel area) to provide the voltage demanded by the EC process. This makes

the cell less appropriate for the task. Methane production follows the same logic with 9.5 % and 6.2% in efficiency.

The preferable path for methane production showed to be dependent on the finality and FTS conditions. In other words, if it was possible to use syngas the same way we use methane, despite methane having higher heating values, the efficiency of the process makes more difference and it would be preferable to use syngas. If the intention is to obtain methane, the 2-step pathway is preferable only if FTS process conditions, temperature and pressure, are low (close and above 350 °C and 10-15 atm). These conditions allow a process efficiency close to 100% and small process cost, which is mainly influenced by the pressure. The process considers Ni catalysts because it is the material with the best compromise between selectivity, activity and cost/abundance.

We have also calculated the installation area required to satisfy an average European household. The most promising results are the ones regarding the 2-step process with Perovskite/Si tandem cells, which would only require 55 m^2. Some improvements in the PV-EC systems still need to be made, mainly in solar efficiencies which are still below 30%, so we can implement such system at the roof of our house, which in average has 31.5 ± 10.1 m^2.

5 Future Perspectives

Despite many works on H_2 production, there are few complete reports regarding methane or syngas production, which makes it difficult to develop simulation works like the present one. This reflects the difference in maturity of both technologies. Electrolytic H_2 production is a commercial technology, whereas syngas/CH_4 produced by co-electrolysis of CO_2 and water it is still in research phase. It would be interesting to see a work that would approach both the experimental and simulation part in order to improve models and verify some of our predictions. Electrochemical models should be improved in order to predict reaction saturation and get closer to reality at low operating voltages. Finally, it would be interesting to study the implementation of a CO_2 capturing system (from the atmosphere) that could be upstream used with the studied PV-EC system, making the fuel producing process even more self-sustainable.

6 References

[1] Energias Renovables, “Solar fuels.” [Online]. Available: https://www.energias-renovables.com/movilidad-1/toyota-quiere-obtener-hidrogeno-a-partir-del-20190214. [Accessed: 05-Sep-2019].

[2] European Commission, “Energy performance of buildings.” [Online]. Available: https://ec.europa.eu/energy/en/topics/energy-efficiency/energy-performance-of-buildings. [Accessed: 14-Jun-2019].

[3] European Commission, “Heating and Cooling.” [Online]. Available: https://ec.europa.eu/energy/en/topics/energy-efficiency/heating-and-cooling. [Accessed: 14-Jun-2019].

[4] S. Styring, “Artificial photosynthesis for solar fuels,” *Faraday Discuss.*, vol. 155, pp. 357–376, 2012.

[5] I. Ganesh, “Electrochemical conversion of carbon dioxide into renewable fuel chemicals - The role of nanomaterials and the commercialization,” *Renew. Sustain. Energy Rev.*, vol. 59, pp. 1269–1297, 2016.

[6] M. A. Modestino and S. Haussener, “An Integrated Device View on Photo-Electrochemical Solar-Hydrogen Generation,” *Annu. Rev. Chem. Biomol. Eng.*, vol. 6, no. 1, pp. 13–34, 2015.

[7] F. Vieira, B. Sarmento, A. S. Reis-MAchado, J. Falcão, M. J. Carvalho, E. Fortunato, R. Martins, and M. J. Mendes, “Prediction of sunlight-driven CO2 conversion : Producing methane from photovoltaics , and full system design for single-house application,” *Mater. Today Energy*, vol. 14, pp. 1–10, 2019.

[8] K. Manthiram, B. J. Beberwyck, and A. P. Alivisatos, “Enhanced electrochemical methanation of carbon dioxide with a dispersible nanoscale copper catalyst,” *J. Am. Chem. Soc.*, vol. 136, no. 38, pp. 13319–13325, 2014.

[9] R. B. Kutz, Q. Chen, H. Yang, S. D. Sajjad, Z. Liu, and I. R. Masel, “Sustainion Imidazolium-Functionalized Polymers for Carbon Dioxide Electrolysis,” *Energy Technol.*, vol. 5, no. 6, pp. 929–936, 2017.

[10] T. Duong, Y. L. Wu, H. Shen, J. Peng, X. Fu, D. Jacobs, E. C. Wang, T. C. Kho, K. C. Fong, M. Stocks, E. Franklin, A. Blakers, N. Zin, K. McIntosh, W. Li, Y. B. Cheng, T. P. White, K. Weber, and K. Catchpole, “Rubidium Multication Perovskite with Optimized Bandgap for Perovskite-Silicon Tandem with over 26% Efficiency,” *Adv. Energy Mater.*, vol. 7, no. 14, pp. 1–11, 2017.

[11] M. T. Hörantner and H. J. Snaith, “Predicting and optimising the energy yield of perovskite-on-silicon tandem solar cells under real world conditions,” *Energy Environ. Sci.*, vol. 10, no. 9, pp. 1983–1993, 2017.

[12] M. Chapa, M. F. Alexandre, M. J. Mendes, H. Águas, E. Fortunato, and R. Martins, “All-Thin-Film Perovskite/C-Si Four-Terminal Tandems: Interlayer and Intermediate Contacts Optimization,” *ACS Appl. Energy Mater.*, vol. 2, no. 6, pp. 3979–3985, 2019.

[13] M. Alexandre, M. Chapa, S. Haque, M. J. Mendes, H. Águas, E. Fortunato, and R. Martins, “Optimum Luminescent Down-Shifting Properties for High Efficiency and Stable Perovskite Solar Cells,” *ACS Appl. Energy Mater.*, vol. 2, no. 4, pp. 2930–2938, 2019.

[14] M. Schreier, F. Héroguel, L. Steier, S. Ahmad, J. S. Luterbacher, M. T. Mayer, J. Luo, and M. Grätzel, “Solar conversion of CO2 to CO using Earth-abundant electrocatalysts prepared by atomic layer modification of CuO,” *Nat. Energy*, vol. 2, no. 7, p. 17087, 2017.

[15] D. M. Weekes, D. A. Salvatore, A. Reyes, A. Huang, and C. P. Berlinguette, “Electrolytic CO2 Reduction in a Flow Cell,” *Acc. Chem. Res.*, vol. 51, no. 4, pp. 910–918, 2018.

[16] T. Pardal, S. Messias, M. Sousa, A. S. R. Machado, C. M. Rangel, D. Nunes, J. V. Pinto, R. Martins, and M. N. Da Ponte, “Syngas production by electrochemical CO2 reduction in an ionic liquid

based-electrolyte," *J. CO2 Util.*, vol. 18, pp. 62–72, 2017.
[17] S. Messias, M. M. Sousa, M. Nunes da Ponte, C. M. Rangel, T. Pardal, and A. S. Reis Machado, "Electrochemical production of syngas from CO2 at pressures up to 30 bar in electrolytes containing ionic liquid," *React. Chem. Eng.*, 2019.
[18] J. Qiao, Y. Liu, and J. Zhang, "Electrochemical Reduction of Carbon Dioxide: Fundamentals and Technologies," Vancouver, British Columbia, Canada.: CRC Press Taylor & Francis Group, 2016, pp. 47–154.
[19] R. I. Masel, Z. Liu, Q. Chen, R. Kutz, H. Yang, K. Lewinski, M. Kaplun, S. Luopa, and D. R. Lutz, "Electrochemical generation of syngas from water and carbon dioxide at industrially important rates," *Biochem. Pharmacol.*, vol. 15, pp. 50–56, 2016.
[20] M. R. Singh, E. L. Clark, and A. T. Bell, "Effects of electrolyte, catalyst, and membrane composition and operating conditions on the performance of solar-driven electrochemical reduction of carbon dioxide.," *Phys. Chem. Chem. Phys.*, vol. 17, no. 29, pp. 18924–36, Jul. 2015.
[21] W. Ma, E. L. Kugler, J. Wright, D. B. Dadyburjor, C. Engineering, W. Virginia, V. Uni, W. Virginia, R. V May, V. Re, M. Recei, and V. September, "Mo - Fe Catalysts Supported on Activated Carbon for Synthesis of Liquid Fuels by the Fischer - Tropsch Process : Effect of Mo Addition on Reducibility , Activity , and Hydrocarbon Selectivity," no. 20, pp. 2299–2307, 2006.
[22] S. Mousavi, A. Zamaniyan, M. Irani, and M. Rashidzadeh, "Generalized kinetic model for iron and cobalt based Fischer-Tropsch synthesis catalysts: Review and model evaluation," *Appl. Catal. A Gen.*, vol. 506, pp. 57–66, 2015.
[23] J. Gao, Y. Wang, Y. Ping, D. Hu, G. Xu, and F. Su, "A thermodynamic analysis of methanation reactions of carbon oxides for the production of synthetic natural gas," *RSC Adv.*, vol. 2, pp. 2358–2368, 2012.
[24] S. Rönsch, J. Köchermann, J. Schneider, and S. Matthischke, "Global Reaction Kinetics of CO and CO2 Methanation for Dynamic Process Modeling," *Chem. Eng. Technol.*, vol. 39, no. 2, pp. 208–218, 2016.
[25] S. Rönsch, J. Schneider, S. Matthischke, M. Schlüter, M. Götz, J. Lefebvre, P. Prabhakaran, and S. Bajohr, "Review on methanation – From fundamentals to current projects," vol. 166, pp. 276–296, 2016.
[26] C. H. Bartholomew, "RECENT TECHNOLOGICAL DEVELOPMENTS IN FISCHER-TROPSCH CATALYSIS Calvin H. BARTHOLOMEW," *Catal. Letters*, vol. 7, pp. 303–315, 1990.
[27] F. Vieira, "Sunlight-driven CO2 Conversion : Producing Methane with Photovoltaics," Nova de Lisboa, Faculdade de Ciência e Tecnologias, 2018.
[28] Eurogas and GasNaturally, "Gas: Europe's smart choice for heating." [Online]. Available: https://gasnaturally.eu/mediaroom/gas-europes-smart-choice-for-heating/. [Accessed: 19-Jun-2019].
[29] GERG, marcogaz, and eurogas, "Gas : the right choice for heating in Europe," 2014. [Online]. Available: http://www.gerg.eu/publications/publications. [Accessed: 19-Jun-2019].
[30] C. Delacourt and J. Newman, "Mathematical Modeling of CO2 Reduction to CO in Aqueous Electrolytes II. Study of an Electrolysis Cell Making Syngas (CO+H2) from CO2 and H2O Reduction at Room Temperature," *J. Electrochem. Soc.*, vol. 157, no. 12, p. B1911, 2010.
[31] A. Awasthi, K. Scott, and S. Basu, "Dynamic modeling and simulation of a proton exchange membrane electrolyzer for hydrogen production," *Int. J. Hydrogen Energy*, vol. 36, no. 22, pp. 14779–14786, 2011.
[32] S. Sawada, T. Yamaki, T. Maeno, M. Asano, A. Suzuki, T. Terai, and Y. Maekawa, "Solid polymer electrolyte water electrolysis systems for hydrogen production based on our newly developed membranes, Part I: Analysis of voltage-current characteristics," *Prog. Nucl. Energy*, vol. 50, no. 2–6, pp. 443–448, 2008.
[33] M. Carmo, D. L. Fritz, J. Mergel, and D. Stolten, "A comprehensive review on PEM water electrolysis," *Int. J. Hydrogen Energy*, vol. 38, no. 12, pp. 4901–4934, 2013.

[34] P. Choi, D. G. Bessarabov, and R. Datta, “A simple model for solid polymer electrolyte (SPE) water electrolysis,” *Solid State Ionics*, vol. 175, no. 1–4, pp. 535–539, 2004.
[35] T. Thampan, S. Malhotra, J. Zhang, and R. Datta, “PEM fuel cell as a membrane reactor,” *Catal. Today*, vol. 67, no. 1–3, pp. 15–32, 2001.
[36] J. Newman, K. E., and Thomas-Alyea, “Electrochemical Systems,” Third., John Wiley & Sons, Inc Publication, 2004, pp. 1–26.
[37] P. Yadav and S. Basu, “An Integrated Device for Converting Water, Carbon Dioxide and Light into Electricity and Organics,” *J. Electrochem. Soc.*, vol. 164, no. 11, pp. E3406–E3417, 2017.
[38] L. Liu, W. Liu, X. Zhang, and J. Ingenhoff, “Research on the novel explicit model for photovoltaic I-V characteristic of the single diode model under different splitting spectrum,” *Results Phys.*, vol. 12, pp. 662–672, 2019.
[39] S. Karmalkar and S. Haneefa, “A physically based explicit J-V model of a solar cell for simple design calculations,” *IEEE Electron Device Lett.*, vol. 29, no. 5, pp. 449–451, 2008.
[40] A. J. Martín, G. O. Larrazábal, and J. Pérez-Ramírez, “Towards sustainable fuels and chemicals through the electrochemical reduction of CO 2 : lessons from water electrolysis,” *Green Chem.*, vol. 17, no. 12, pp. 5114–5130, 2015.
[41] S. Sangwine, *Electronic Components and Technologies*, Third. CRC Press, 2007.
[42] Cool Roof Rating Council, “Effect of Rooftop Exposure on Conduit Ambient Temperatures Presentation.” Reno Nevada, p. 50, 2011.
[43] Engineering ToolBox, “Fuels - Higher and Lower Calorific Values,” 2003. [Online]. Available: https://www.engineeringtoolbox.com/fuels-higher-calorific-values-d_169.html. [Accessed: 16-Jun-2019].
[44] Engineering ToolBox, “Hydrogen - Specific Heat,” 2005. [Online]. Available: https://www.engineeringtoolbox.com/hydrogen-d_976.html. [Accessed: 26-Jun-2019].
[45] Engineering ToolBox, “Carbon Monoxide - Specific Heat,” 2005. [Online]. Available: https://www.engineeringtoolbox.com/carbon-monoxide-d_975.html. [Accessed: 16-Jun-2019].
[46] BP, “BP Statistical Review of World Energy,” 2018.
[47] S. Izquierdo, M. Rodrigues, and N. Fueyo, “A method for estimating the geographical distribution of the available roof surface area for large-scale photovoltaic energy-potential evaluations,” vol. 82, pp. 929–939, 2008.
[48] eurostat, “Average household size, 2008 and 2018 (average number of persons in private households),” 2019. [Online]. Available: https://ec.europa.eu/eurostat/statistics-explained/index.php?title=File:Average_household_size,_2008_and_2018_(average_number_of_persons_in_private_households)_new.png. [Accessed: 10-Aug-2019].

Appendix I

Solar (Perovskite/Si tandem or mono-Si) to fuel (methane or syngas) total efficiency with and without DCDC converter

The plots are labelled according to the type of fuel and cell as follows: "fuel" _ "solar cell type" _ "proportion of CO in output fuel" _ "type of thermal coupling". The third parameter is empty (for CH4 production) and equal to the "fuel" when there is only H_2 or only CO production.

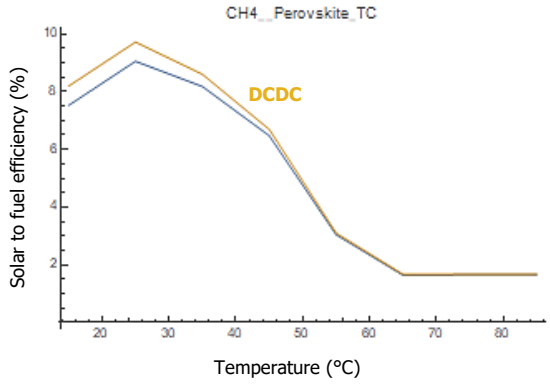

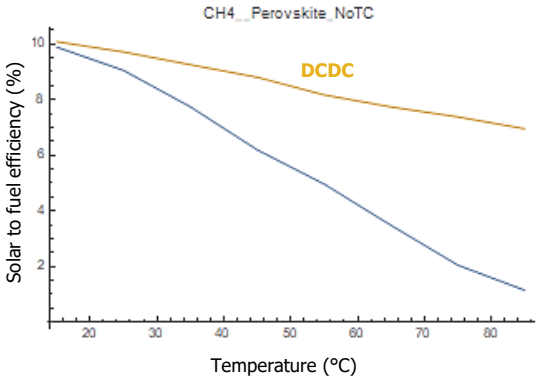

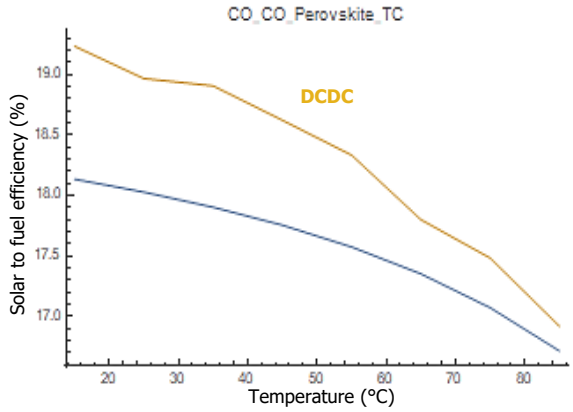

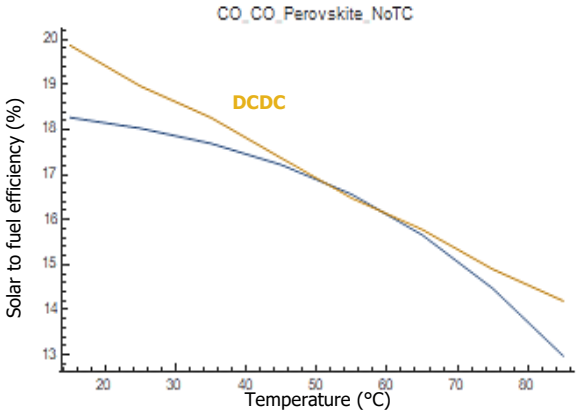

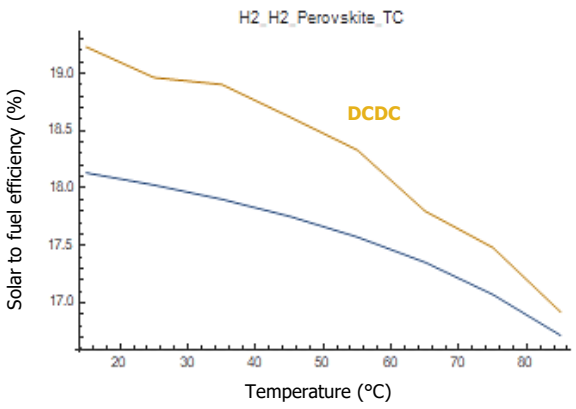

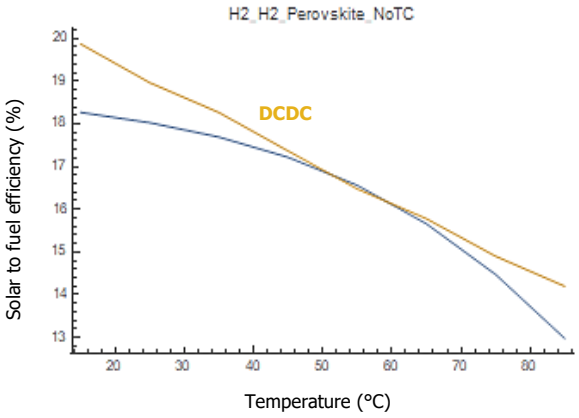

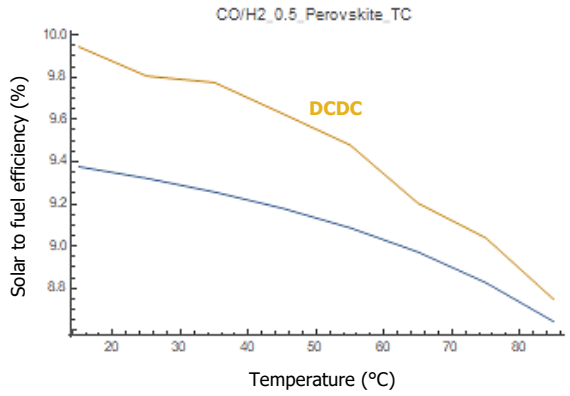
CO/H2_0.5_Perovskite_TC
DCDC
Solar to fuel efficiency (%)
Temperature (°C)

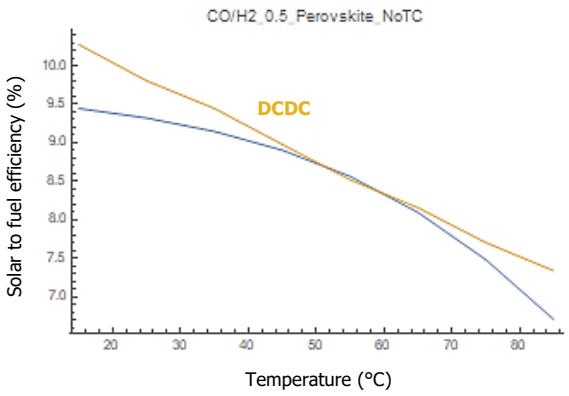
CO/H2_0.5_Perovskite_NoTC
DCDC
Solar to fuel efficiency (%)
Temperature (°C)

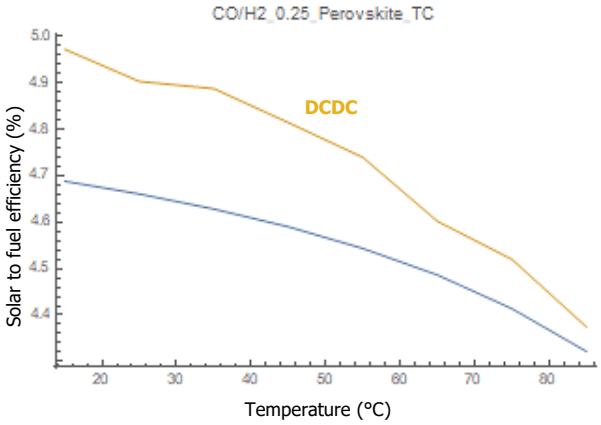
CO/H2_0.25_Perovskite_TC
DCDC
Solar to fuel efficiency (%)
Temperature (°C)

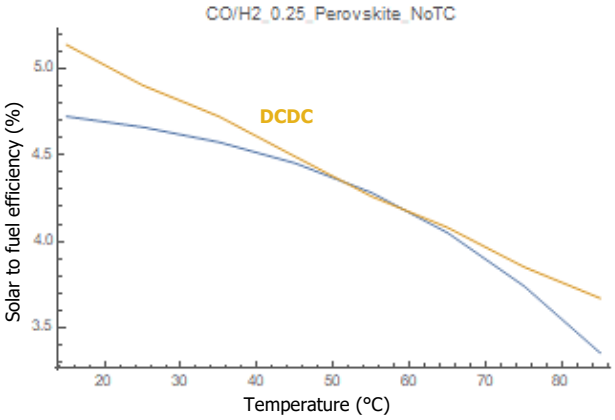
CO/H2_0.25_Perovskite_NoTC
DCDC
Solar to fuel efficiency (%)
Temperature (°C)

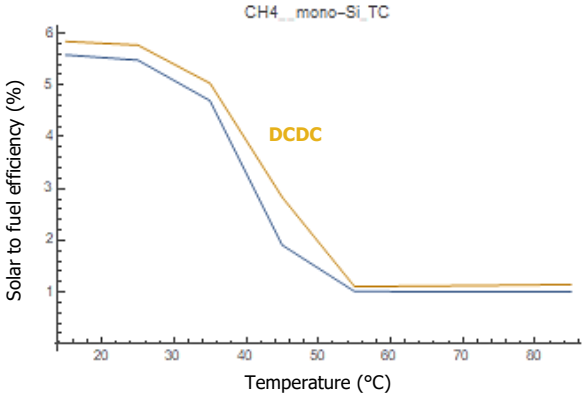
CH4__mono-Si_TC
DCDC
Solar to fuel efficiency (%)
Temperature (°C)

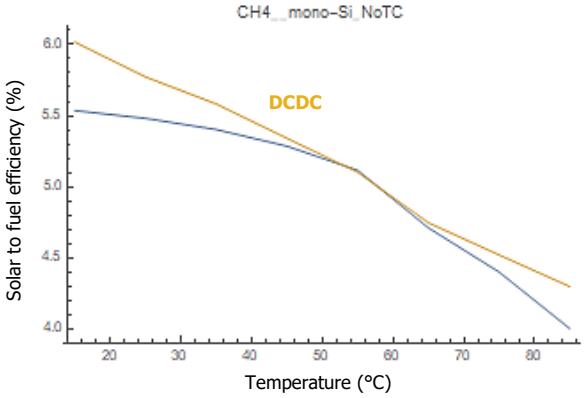
CH4__mono-Si_NoTC
DCDC
Solar to fuel efficiency (%)
Temperature (°C)

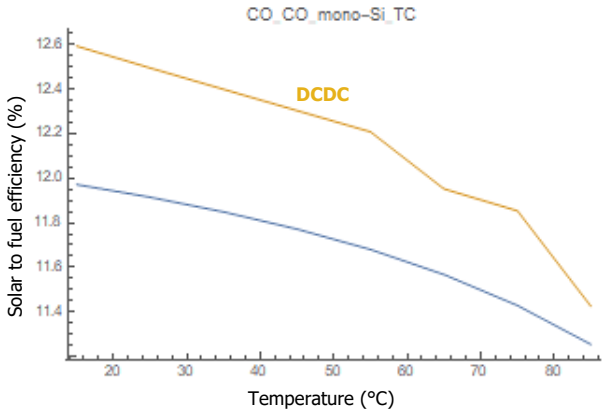
CO_CO_mono-Si_TC
DCDC
Solar to fuel efficiency (%)
Temperature (°C)

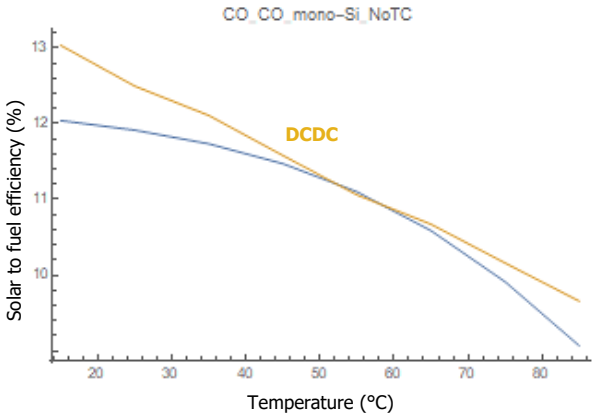
CO_CO_mono-Si_NoTC
DCDC
Solar to fuel efficiency (%)
Temperature (°C)

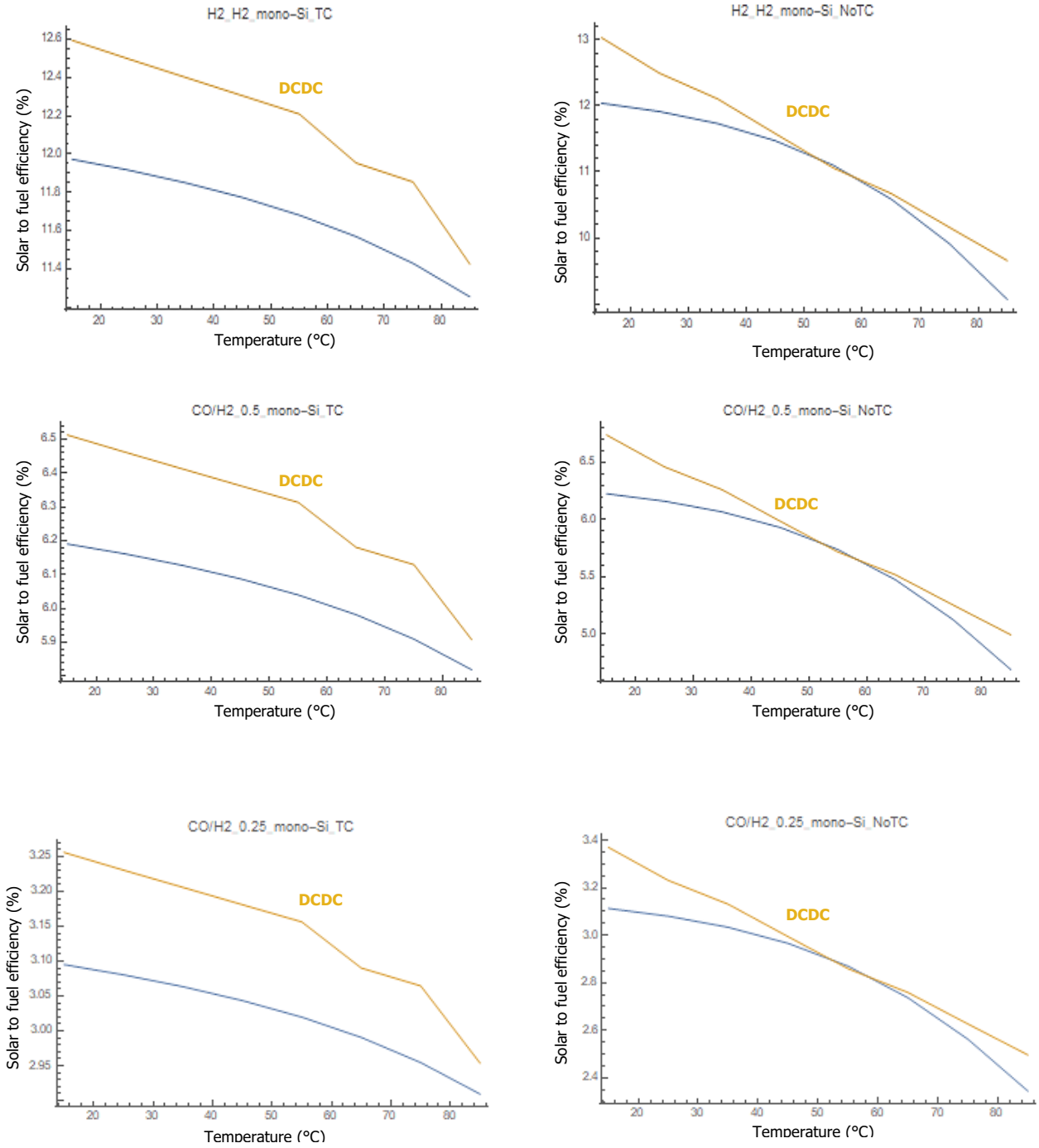

Figure A. 1 - total efficiency as a function of temperature for comparison of the system with and without DCDC converter.

Appendix II

Production over area ratio with and without DCDC converter

The plots are labelled according to the type of fuel and cell as follows: "fuel" _ "solar cell type" _ "proportion of CO in output fuel" _ "type of thermal coupling". The third parameter is empty (for CH4 production) and equal to the "fuel" when there is only H_2 or only CO production.

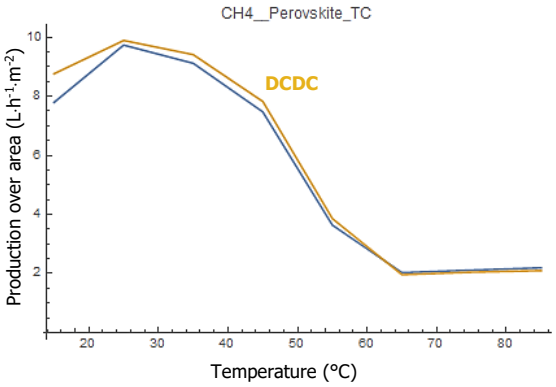

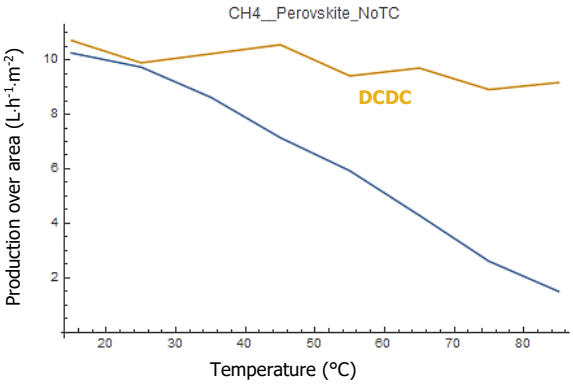

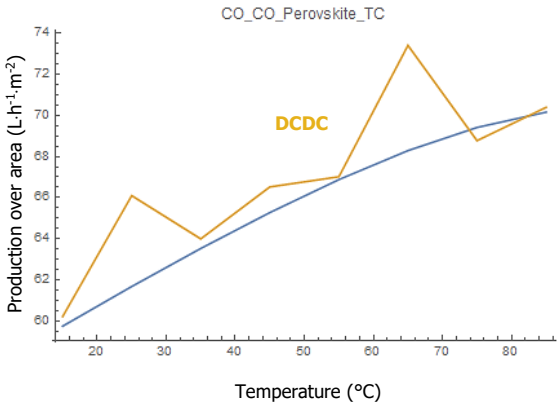

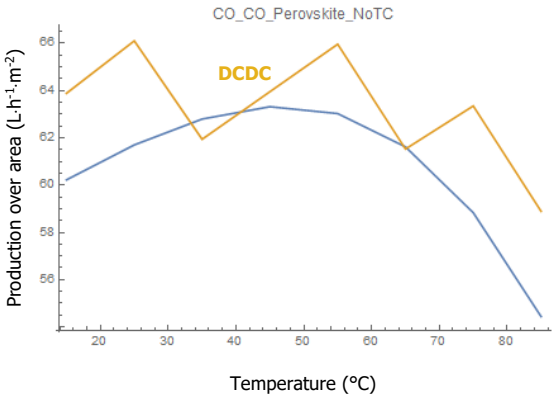

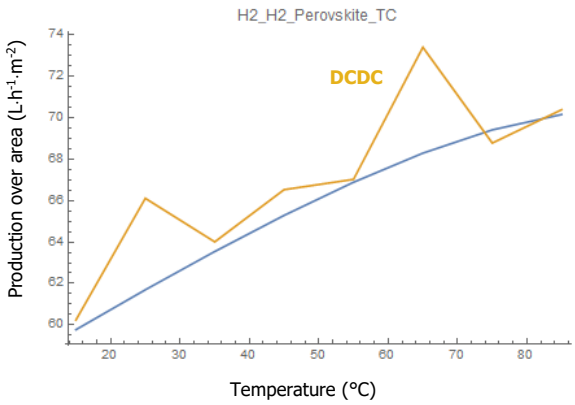

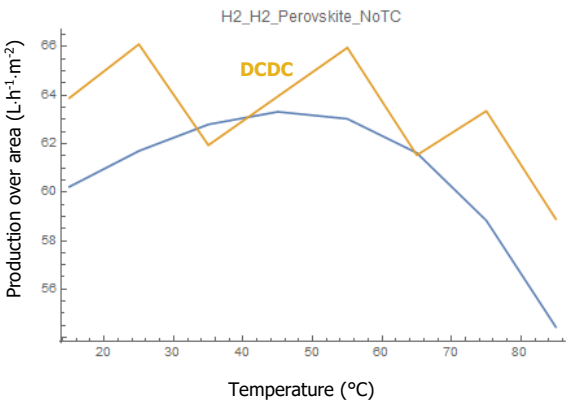

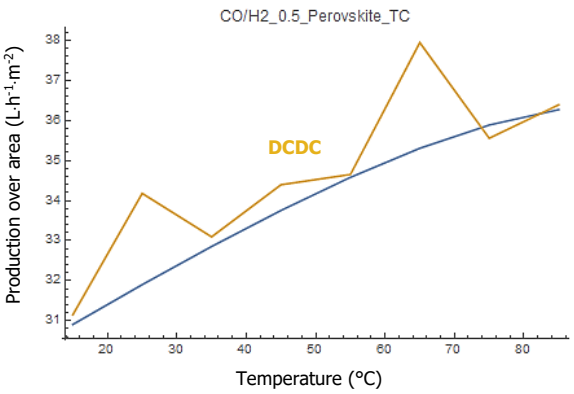
CO/H2_0.5_Perovskite_TC
DCDC
Production over area (L·h-1·m-2)
Temperature (°C)

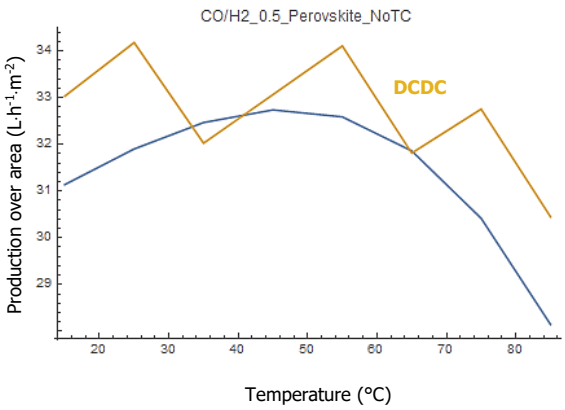
CO/H2_0.5_Perovskite_NoTC
DCDC
Production over area (L·h-1·m-2)
Temperature (°C)

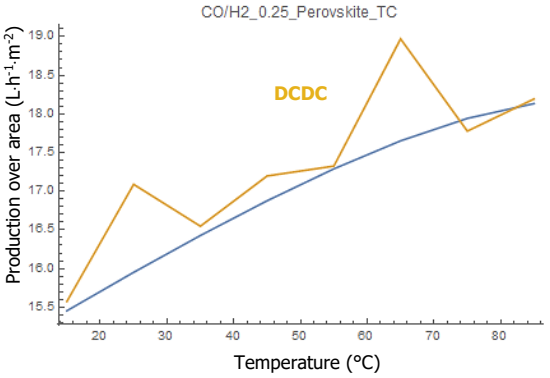
CO/H2_0.25_Perovskite_TC
DCDC
Production over area (L·h-1·m-2)
Temperature (°C)

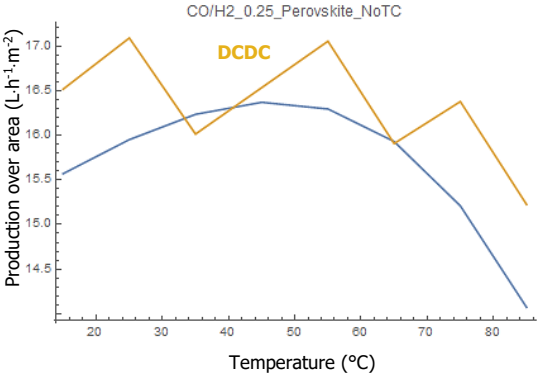
CO/H2_0.25_Perovskite_NoTC
DCDC
Production over area (L·h-1·m-2)
Temperature (°C)

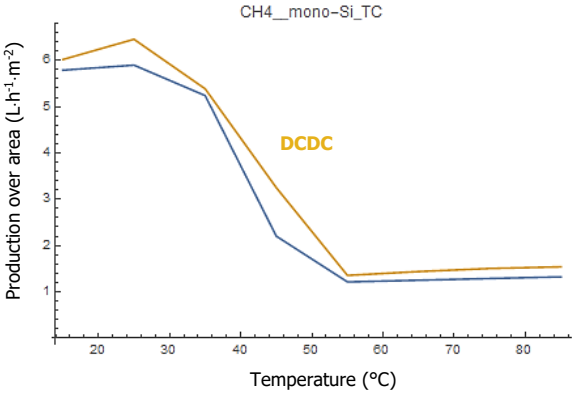
CH4__mono-Si_TC
DCDC
Production over area (L·h-1·m-2)
Temperature (°C)

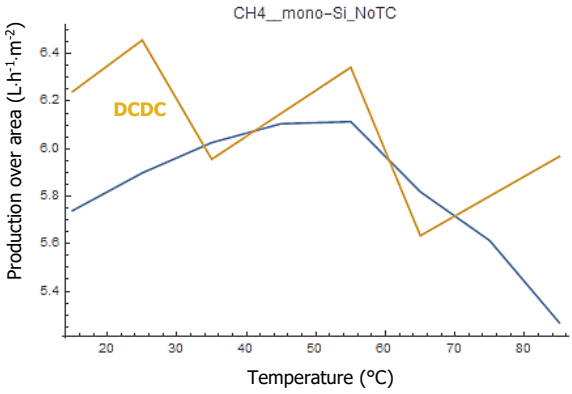
CH4__mono-Si_NoTC
DCDC
Production over area (L·h-1·m-2)
Temperature (°C)

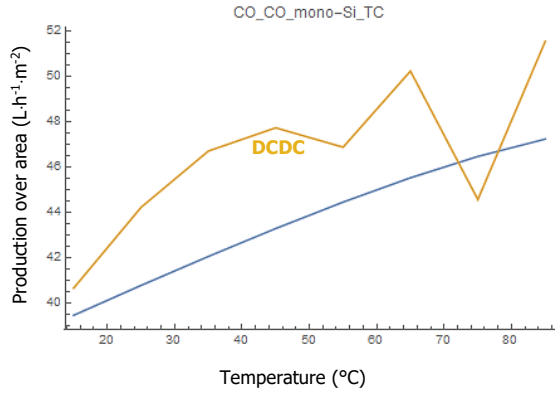
CO_CO_mono-Si_TC
DCDC
Production over area (L·h-1·m-2)
Temperature (°C)

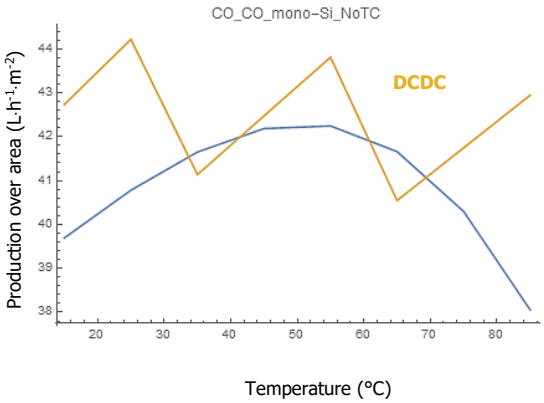
CO_CO_mono-Si_NoTC
DCDC
Production over area (L·h-1·m-2)
Temperature (°C)

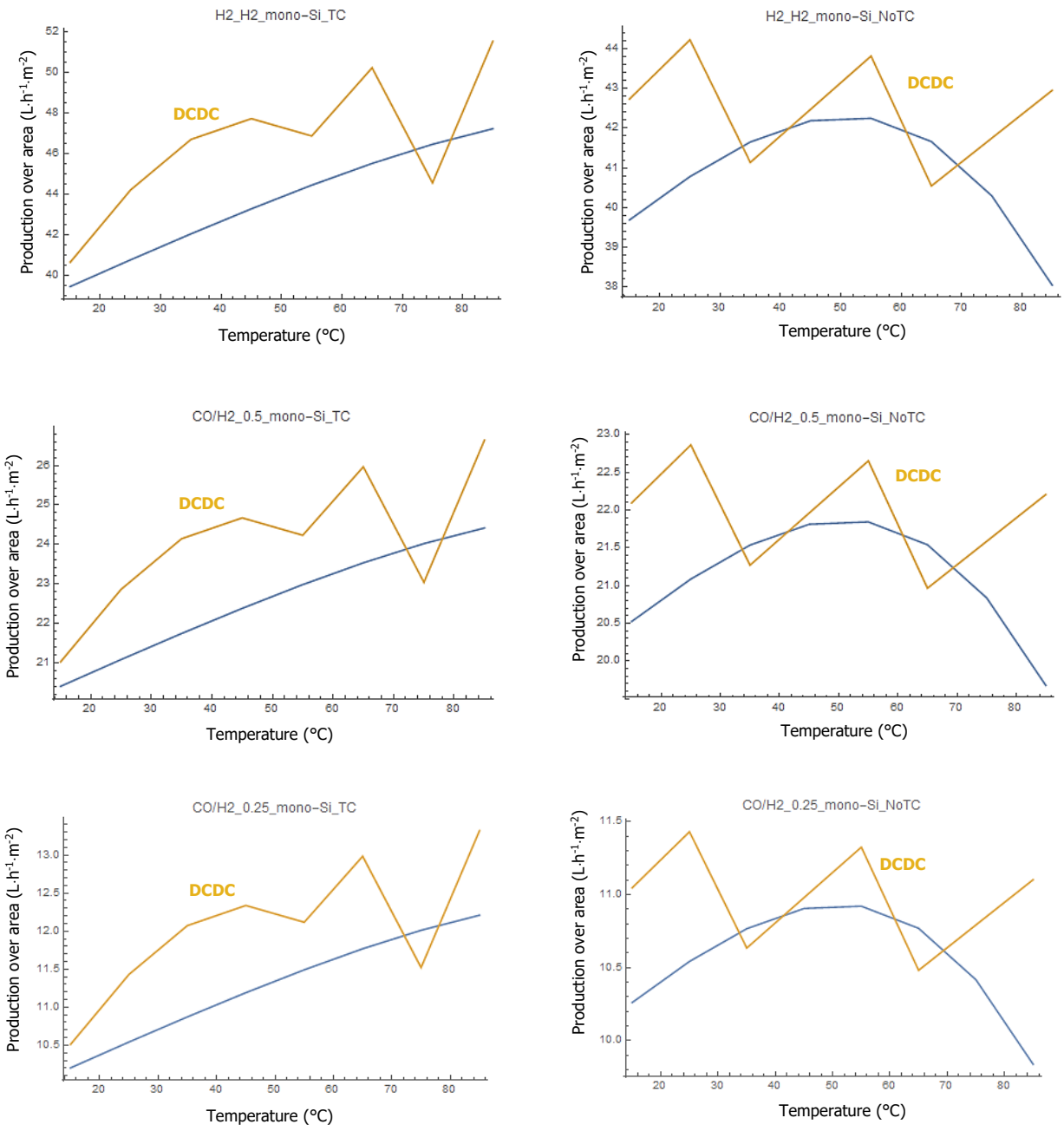

Figure A. 2 - production over area ratio as a function of temperature for comparison of the system with and without DCDC converter.

Annex I

SUNPOWER mono-Si solar cells Datasheet

SUNPOWER

B50 SOLAR CELL

MONO CRYSTALLINE SILICON

Electrical Characteristics of Typical Cell at Standard Test Conditions (STC)

STC: 1000W/m², AM 1.5g and cell temp 25°C

Bin	Pmpp (Wpl	Eff. (%)	Vmpp (V)	Impp (A)	Voc (V)	Isc (A)
G	2.97	20.0	0.557	5.33	0.664	5.72
H	3.04	20.4	0.563	5.39	0.668	5.76
I	3.10	20.8	0.568	5.45	0.671	5.82
J	3.15	21.2	0.571	5.51	0.673	5.87

All Electrical Characteristics parameters are nominal
Unlaminated Cell Temperature Coefficients
Voltage: -1.8 mV / °C Power: -0.32% / °C

Positive Electrical Ground

Modules and systems produced using these cells must be configured as "positive ground systems".

TYPICAL I-V CURVE

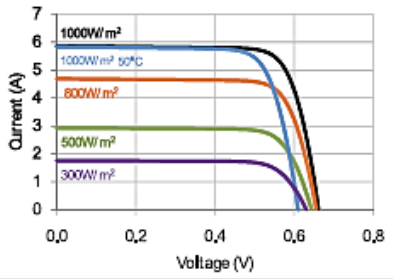

SPECTRAL RESPONSE

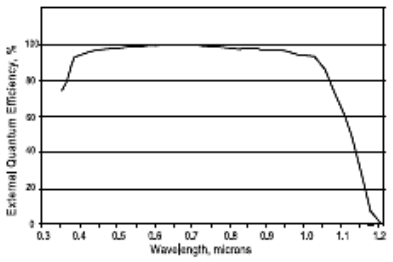

Physical Characteristics

Construction:	All back contact
Dimensions:	125mm x 125mm (nominal)
Thickness:	165µm ± 40µm
Diameter:	150mm (nominal)

Cell and Bond Pad Dimensions

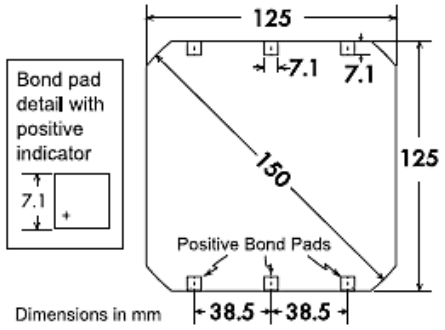

Bond pad area dimensions are 7.1mm x 7.1mm
Positive pole bond pad side has "+" indicator on leftmost and rightmost bond pads.

Interconnect Tab and Process Recommendations

Tin plated copper interconnect. Compatible with lead free process.

Packaging

Cells are packed in boxes of 1,200 each; grouped in shrink-wrapped stacks of 150 with interleaving. Twelve boxes are packed in a water-resistant "Master Carton" containing 14,400 cells suitable for air transport.

Interconnect tabs are packaged in boxes of 1,200 each.

About SunPower

SunPower designs, manufactures, and delivers high-performance solar electric technology worldwide. Our high-efficiency solar cells generate up to 50 percent more power than conventional solar cells. Our high-performance solar panels, roof tiles, and trackers deliver significantly more energy than competing systems.

sunpowercorp.com

Figure A. 3 - Datasheet for B50 Solar Cell by SUNPOWER.

Annex II

Electrochemical curves (JV) used for methane electrolyser

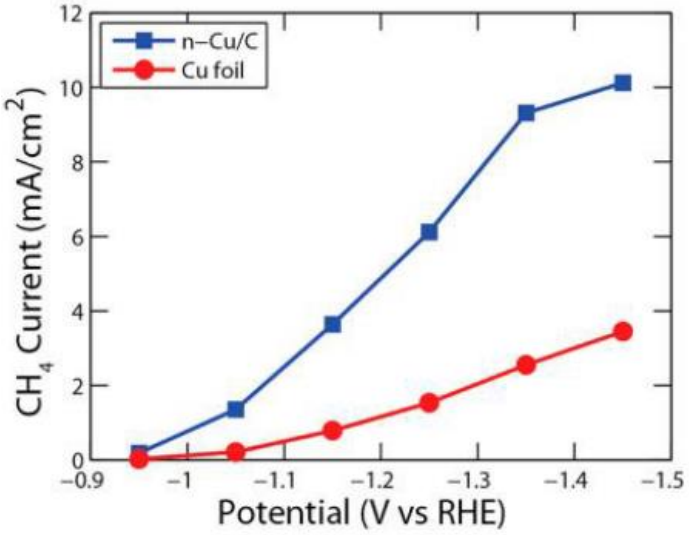

Figure A. 4 – EC current density versus Voltage (vs RHE) from Manthiram et al. work [7].

Annex III

Electrochemical curves (JV) used for syngas electrolyser

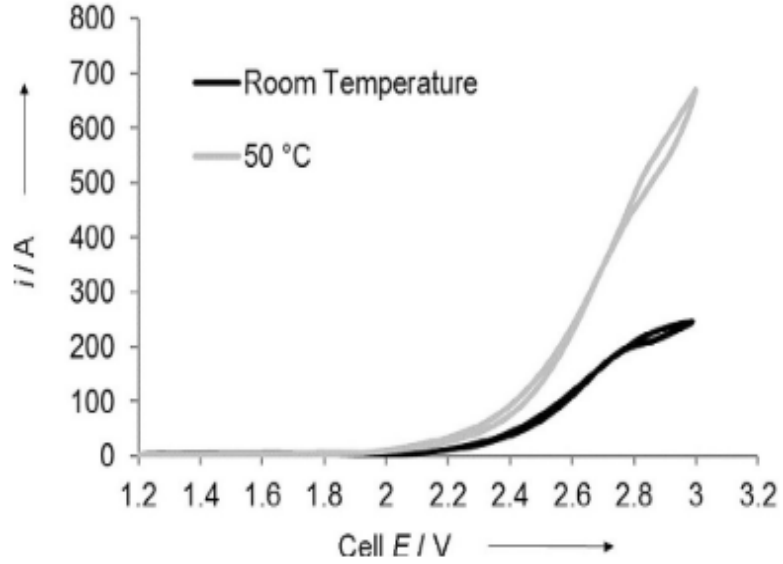

Figure A. 5 – EC current density versus Voltage (vs RHE) at different temperatures from Kutz et al. work [8].